Neural Dynamics of Single Units in Rat's Agranular Medial and Agranular Lateral Areas during Learning of a Directional Choice Task

by

Yuan Yuan

A Dissertation Presented in Partial Fulfillment
of the Requirement for the Degree
Doctor of Philosophy

Approved February 2014 by the
Graduate Supervisory Committee:

Jennie Si, Chair
Christopher Buneo
Marco Santello
Junseok Chae

ARIZONA STATE UNIVERSITY

May 2014

ABSTRACT

Learning by trial-and-error requires retrospective information that whether a past action resulted in a rewarded outcome. Previous outcome in turn may provide information to guide future behavioral adjustment. But the specific contribution of this information to learning a task and the neural representations during the trial-and-error learning process is not well understood. In this dissertation, such learning is analyzed by means of single unit neural recordings in the rats' motor agranular medial (AGm) and agranular lateral (AGl) while the rats learned to perform a directional choice task. Multichannel chronic recordings using implanted microelectrodes in the rat's brain were essential to this study. Also for fundamental scientific investigations in general and for some applications such as brain machine interface, the recorded neural waveforms need to be analyzed first to identify neural action potentials as basic computing units. Prior to analyzing and modeling the recorded neural signals, this dissertation proposes an advanced spike sorting system, the M-Sorter, to extract the action potentials from raw neural waveforms. The M-Sorter shows better or comparable performance compared with two other popular spike sorters under automatic mode. With the sorted action potentials in place, neuronal activity in the AGm and AGl areas in rats during learning of a directional choice task is examined. Systematic analyses suggest that rats neural activity in AGm and AGl was modulated by previous trial outcomes during learning. Single unit based neural dynamics during task learning are described in detail in the dissertation. Furthermore, the differences in neural modulation between fast and slow learning rats were compared. The results show that the level of neural modulation of previous trial outcome is different in fast and slow learning rats which may in turn suggest an important role of previous trial outcome encoding in learning.

DEDICATION

To Dr. Jennie Si for her unwavering support, encouragement and supervision over the years.

ACKNOWLEDGEMENTS

Over the past five years I have received support and encouragement from a great number of individuals. I would like to thank my dissertation committee of Dr. Christopher Buneo, Dr. Marco Santello, and Dr. Junseok Chae for their support.

I would like to thank Dr. Steven P. Wise for reading and editing a previous version of the materials in Chapters 3 and 4 of the Dissertation. I would also like to thank Dr. Jun Shen for his advise and help during the experiment by providing ideas and parts for the design and implementation of the experimental apparatus.

During data collection and manuscript writing Hongwei Mao spent countless hours listening to me talking about my research. Bing Cheng, Sijia Wang and Weichao Ma provided timely encouragement and insights. The lab assistants in our NeuroControl Lab, Rachel Austin, Amelia Spinrad, Eric Smith, Emily Herring, and Taylor Ketchum, provided technical support.

I would also like to thank my best friend Jinjin Li who has been side-by-side with me and has kept my sanity in check through these difficult years.

Finally, thanks to my family for all their love and encouragement. For my parents who raised me with unconditional love and supported me in all my pursuits. And most of all for my husband Ge Tan for his patience, understanding and encouraging.

The dissertation work was supported in part by the National Science Foundation under Grants ECS-0702057 and ECS-1002391.

TABLE OF CONTENTS

CHAPTER Page

CHAPTER Page

LIST OF FIGURES

Figure Page

Chapter 1

INTRODUCTION

One fundamental question in the field of neuroscience is the elucidation of neural mechanisms underlying alternations in behavior, such as cognitive learning. Multiple brain areas are involved in learning. In the frontal cortex, recent researches find that motor cortex plays important roles in high level cognition. Especially in experiments which uses stereotypical movement as effector, they may be good candidates to study behavioral changes. In recent decades, advancement in single unit recordings facilitates research in this area. Spike detection and classification are fundamental and important topics in any chronic recording studies in neuroscience. This dissertation uses the state-of-the-art electrophysiology to study the developmental mechanisms of behavior in non-human animals. Specifically, I seek to analyze the behavioral changes and patterns of neural activities among identifiable populations of neurons using a properly designed behavioral protocol.

The first contribution of this dissertation is implementation of an advanced spike detection and classification algorithm. Neural spike detection and classification, or spike sorting, is the first and a critical step prior to any single unit based neuroscientific studies and applications. A good spike sorter is usually characterized by high detection and classification accuracy, robust to changes in signal-to-noise ratio, objectivity in detection results or less user dependency, and real-time applicability. Here I present an automatic and robust spike detection and classification system, the M-Sorter, based on the multiple correlation of wavelet coefficients (MCWC) detection algorithm in conjunction with template matching for classification. Unlike many existing spike sorters that make use of a series of complex spike classifiers to deal with the challenges resulted from a low performance spike detector, the M-Sorter

relies on a high performance yet computationally efficient detection algorithm and thus a simple classifier suffices to generate high quality spike sorting results. In this dissertation I provide step by step implementation procedures of the M-Sorter. The M-Sorter has been compared with other popular spike sorters and shows equivalent or better performance over artificial and real neural data sets.

The second contribution of this dissertation is functional analysis in rats motor cortical areas. The outcomes that result from previous behavior affects future choices in several ways, but the neural mechanisms for these effects remain to be determined. Previous studies have shown that the agranular lateral (AGl) and agranular medial (AGm) areas of the rat frontal cortex, which correspond to the primary motor cortex and one of the nonprimary motor areas in primates, respectively, are involved in the learning and selection of action. Here I describe the activity of single neurons in AGl and AGm as rats learn to perform a directional choice task. The analysis shows that single-cell activity in AGl and AGm is modulated by the outcome of the previous trial. A larger proportion of neurons encode the previous trial's outcome shortly after cue onset than during other time periods of a trial. Most of these neurons have greater firing activity after correct trials than after error trials, a difference that reached its peak during learning, compared to trials before and after learning. The number of neurons encoding the previous trial's outcome correlates positively with performance accuracy. In summary, neurons in both AGl and AGm encode the outcome of the immediately preceding trial, especially during learning, information that might play a role in the successful selection of action based on past experience.

The third contribution of this dissertation is the analysis of neural activity of rats with different characteristics when learning to perform a same directional choice task. The way we learn something new and make decisions are different from individual to individual. But whenever placing a group of individuals on learning the same task,

some master the task faster than others. However there is little literature about the neural mechanism that gives rise to different learning outcomes. I use a rat model aiming to address this very issue. Rats single unit neural activities in the AGm and AGl are recorded while they learn to perform a directional choice task. Fast and slow rats are identified according to their learning behavior. The fast rats start to improve task performance immediately and reached high accuracy within 20 sessions while the slow rats took a longer period to pick up. Also, the fast rats reach accuracy of 70% steadily in fewer sessions compared with the slow rats. The analysis shows a larger number of AGm and AGl neurons encoding previous trial outcome in the trial start period for the fast rats than the slow rats. Furthermore, neurons recorded in fast rats are associated with stronger neural firing rate modulation by previous trial outcome than slow rats. These results suggest that previous trial outcome is correlated with learning speed, which may be a neural mechanism separating fast from slow learning rats.

In this dissertation, Chapter 2 presents the algorithm and performance of M-Sorter, Chapter 3 presents the experimental design of directional choice task, Chapter 4 presents the study of cortical correlates to dynamic learning, and Chapter 5 presents the study of individual difference in learning.

Chapter 2

THE M-SORTER: TOWARDS AN AUTOMATIC AND ROBUST SPIKE DETECTION AND CLASSIFICATION SYSTEM

2.1 Introduction

Neural action potentials, also known as nerve impulses or spikes, play an important role in the study of the central nervous system as they are considered the basic computing units in the brain. Via multichannel arrays of microelectrodes, multiple spiking neurons can be recorded simultaneously from behaving animals. This has provided unprecedented opportunity for neuroscientists to study the brain at a high spatial and temporal resolution. But several challenges need to be overcome. First and foremost, noises from brain tissues, muscle movement of the subject, and other biological and instrumental interferences are inevitable, which contaminate the recorded neural waveforms [2]. Second, identifying real neural spikes from noisy recordings often requires making assumptions about the consistency, shape, and individuality of spike waveforms. This has resulted in many different approaches to spike sorting, which can be supervised or unsupervised as discussed in [3] and [4]. Manual spike sorting is a supervised method, which can be subjective to the user's experience and thus result in significantly variant outcomes [5, 6]. Unsupervised methods, or automatic methods, instead, are generally preferred to avoid the subjectivity and to provide real-time applications such as brain-machine interface.

Spike sorting involves two steps - spike detection and spike classification. Existing automatic approaches to spike sorting usually make use of the simple threshold-crossing detection plus a sophisticated clustering algorithm [4, 7, 8]. Thresholding based detection algorithms [9, 10, 11] typically exploit simple measures such as root mean square (RMS) estimation of the background noise [4, 8]. At the same time,

many powerful clustering methods have been developed and introduced for spike sorting [3, 7, 12]. Existing classification methods for spike sorting include shape based and distribution based algorithms [13], principal components [14], wavelet basis [15], template matching [5, 16, 17, 18], k-means, hierarchical clustering [3, 19], independent component analysis (ICA) [20], fuzzy c-means, and a variety of artificial neural network based unsupervised classification schemes [19].

Simple thresholding is intuitive and easy to implement, however, a proper choice of the threshold level is not straightforward. Too high of a threshold value will likely exclude real spikes buried within background noise, while too low of a threshold value will allow a large number of segments of waveforms to be considered as potential real spikes. To avoid missing detection of real spikes, typically a user selects a low threshold value for spike sorting. This consequently creates a great challenge for waveform feature extraction to be used in many of the above mentioned spike sorters. Some advanced wavelet based detection techniques have been proposed to improve detection accuracy [1, 21, 22]. Some reviews and comparisons of different detection algorithms are available in [1].

In this dissertation, I present a complete spike sorting procedure, namely the M-Sorter. The proposed sorter is based on multiple correlation of wavelet coefficients (MCWC) [1] augmented with thresholding for detection, and template matching for classification. I will show that this approach significantly reduces false positives in the detection step and the overall detection and classification accuracy remains high. As will be demonstrated later, the clustered results of the system are clear, robust to noise, and consistent. Only a few parameters need to be selected and the choices for the parameters are straightforward.

The M-Sorter aims for automatic spike sorting based on waveforms recorded from microwire arrays. It will be shown later in the dissertation that the sorter works

just as well as other sorters if the waveform is of high quality, i.e., the signal-to-noise (SNR) ratio is high. However, the M-Sorter is more effective and easier to use than other methods when the SNR is low, or when the background noise is high. In theory the M-Sorter can be applied to other forms of recorded signals including tetrodes, or even possibly EEG waveforms. However, the wavelet functions may need to be adjusted to reflect the nature of EEG spike characteristics. Some key parameters as will be discussed in this dissertation may need to be adjusted to achieve automated and robust spike sorting.

2.2 Materials and Methods

The M-Sorter consists of three major components as shown in Figure 2.1: template generation, detection, and template matching. In the following, I first introduce the MCWC detection algorithm, and then I introduce each of the three steps and provide a summary of the implementation details as well as insight on parameter selection.

2.2.1 A Brief Overview of the Multiple Correlation of Wavelet Coefficients

The multiple correlation of wavelet coefficients (MCWC) is a high performance spike detection algorithm [1, 23]. As demonstrated, it is characterized by high detection accuracy and low false positives, as well as few free parameters.

Let $x(t)$ be a neural waveform, J be the width of the observation window of the waveform under consideration which is used as the integration interval in the calculation of wavelet coefficients. And let N_J be the number of samples in the observation window J. The wavelet transform of $x(t)$ is defined in (3.1). As can be seen, $Tx(a_i, b_j)$ is a measure of resemblance between the wavelet function $\psi(t)$ and the neural signal $x(t)$ with proper translation and scaling parameters a_i and b_j.

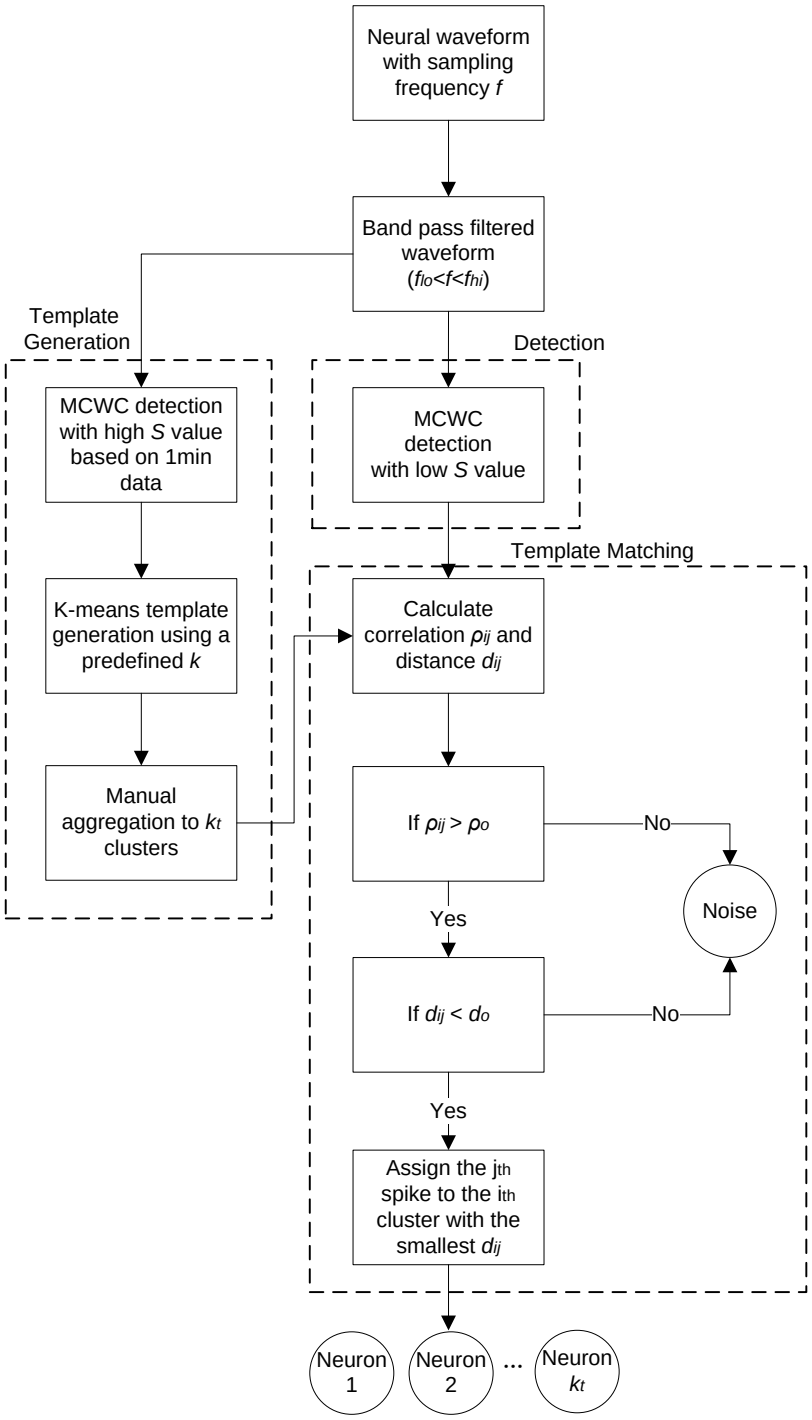

Figure 2.1: Schematic block diagram of the M-Sorter

$$Tx(a_i, b_j) = \int_J x(t) \frac{1}{\sqrt{a_i}} \psi(\frac{t - b_j}{a_i}) dt. \tag{2.1}$$

The two parameters in (3.1) are the time translation factor b and the scale factor a, where b is from a set of N_J components:

$$b \in B = \{0, 1, \cdots, N_J - 1\}. \tag{2.2}$$

The scale factor a, on the other hand, determines the support of the wavelet function. When applied to spike detection in neural recordings, it is chosen between 0.5ms and 1.5ms, i.e.,

$$a \in A = \{0.5, 0.6, \cdots, 1.5\}. \tag{2.3}$$

Given the wide range of wavelet families and their unique features, it is important to select a suitable wavelet function for spike detection. It is noted in [24] that the waveforms of extracellular neural action potentials typically appear mono-phasic, bi-phasic and even tri-phasic. The research by [25] proves that the action potential waveforms of single units in human peripheral nerves also consists of such three kinds of waveforms. Since mono-phasic can be viewed as a building block of bi/tri-phasic waveforms, and the latter can be represented approximately by a superposition of mono-phasic waveforms, in the dissertation I focus on detection using an approximation of a mono-phasic wavelet function. The wavelet function 'coiflets' was selected and used for neural spike detection in [22], [26] and [27]. It is also chosen in MCWC. I choose 'coiflets' based on the following considerations. When the time support of the wavelet function matches the duration of one phase of a neural waveform, the corresponding wavelet transform coefficients become high. As such the mono-phasic wavelet function is also able to generate high wavelet transform coefficients at one

phase of the bi/tri-phasic neural spike waveform. But the waveforms of noise usually do not resemble the wavelet function. Therefore the coefficients from noise have small or close to zero magnitudes. By inspecting waveforms corresponding to high wavelet transform coefficients, I can detect neural spikes even though they may have different phases.

Let $r_S(a_i, b_j)$ be the correlation of wavelet coefficients defined in (3.1) among S sampling scales.

$$r_S(a_i, b_j) = \prod_{k=0}^{S-1} Tx(a_{i+k}, b_j). \tag{2.4}$$

As can be seen from (2.4), $r_S(a_i, b_j)$ is a measure of the strength of resemblance between the wavelet function $\psi(t)$ and the neural signal $x(t)$ with proper translation and scaling parameters a_i and b_j. It does so by first computing the wavelet coefficient $T_x(a_{i+k}, b_j)$, and then enhanced by a verification from multiple sampling scales up to S. As such, $r_S(a_i, b_j)$ defined by (2.4) can potentially produce a more pronounced separation of the coefficients corresponding to neural spikes from those corresponding to noise. Or in other words, this product can potentially reinforce the presence of neural spikes, while it is reduced if $x(t)$ contains mostly noise. The product across multiple levels enhances the robustness of this measure.

Once $r_S(a_i, b_j)$ is obtained, it should be normalized so that the correlation of coefficient measure is still based on the original neural signal scale level, not on different sampling scales. This makes the correlation of coefficient measure comparable with the wavelet coefficient.

Let $r'_S(a_i, b_j)$ be the power normalized correlation of wavelet coefficients defined below,

$$P_{r_S}(a_i) = \sum_{j \in J} r_S(a_i, b_j)^2, \tag{2.5}$$

$$P_{Tx}(a_i) = \sum_{j \in J} Tx(a_i, b_j)^2, \tag{2.6}$$

$$r'_S(a_i, b_j) = r_S(a_i, b_j) \times \sqrt{\frac{P_{Tx}(a_i)}{P_{r_S}(a_i)}}. \tag{2.7}$$

I are now ready for claiming the detection of a spike.

Let H_0 be the null hypothesis that within the window of width J, $x(t)$ does not contain any neural spikes, and let H_1 be the alternative hypothesis that within the window of width J, $x(t)$ contains a spike at b_j. Or in other words, the hypothesis test for the original MCWC [1] is:

H_0: $x(t)$ contains no spikes in the window of width J under consideration.

H_1: $x(t)$ contains a spike at b_j in the window of width J under consideration.

Specifically, H_0 holds, or no spike is detected if

$$|r'_S(a_i, b_j)| \leq |T(a_i, b_j)|, \tag{2.8}$$

and H_1 holds, or a spike is detected, if (2.9) is satisfied,

$$|r'_S(a_i, b_j)| > |T(a_i, b_j)|. \tag{2.9}$$

Let $[t_0, t_1] \in J$ stand for a small sub-interval around b_j such that H_1 holds, and let t_d be the instant of a spike,

$$t_d = \max_{a_i \in [a_0, \cdots, a_{S-1}],\ b_j \in [t_0, t_1]} |r'_S(a_i, b_j)|. \tag{2.10}$$

As shown in [1], the MCWC detection algorithm actually is an adaptive thresholding method. There is one tuning parameter, S, in the MCWC detection algorithm. It automatically adjusts the level of threshold according to the SNR of the neural recording and the tuning parameter, S (Figure 4 in [1]). More discussions on how S affects the detection results can be found in [1].

Once the MCWC has resulted in a pool of carefully detected potential spikes, another simple threshold τ can be applied to eliminate waveforms with magnitude right around the noise floor level, which may take the RMS value of the background noise. However, unlike the detection algorithms based on thresholding, the selection of τ is not as critical and can be easily set at the noise floor level. The introduction of τ is beneficial since it helps remove waveforms with small magnitude and thus increase robustness. Also note that the chosen spike instance t_d in MCWC, as defined in (2.10), is the time instance with the largest power normalized correlation of wavelet coefficients, but t_d may not coincide with the waveform peak value in the time domain. Therefore, the resulted pool of potential spikes may not perfectly align in the time domain. Consequently, this mis-alignment may complicate sorting. Under these considerations, the MCWC hypothesis test is revised for application in the M-Sorter.

The hypothesis test for the revised MCWC is:

H_0: no spike is detected if

$$|r'_S(a_i, b_j)| \leq |T(a_i, b_j)|, \text{ or} \tag{2.11}$$
$$|\max_{b_j \in [t_0, t_1]} x(b_j)| < \tau.$$

H_1: a spike is detected at b_j, if the following conditions are satisfied,

$$|r'_S(a_i, b_j)| > |T(a_i, b_j)|, \text{ and} \tag{2.12}$$
$$|\max_{b_j \in [t_0, t_1]} x(b_j)| \geq \tau.$$

The spike instance is thus chosen at

$$t'_d = \max_{b_j \in [t_0, t_1]} |x(b_j)|. \tag{2.13}$$

Therefore, in the revised hypothesis test, t'_d is chosen at the instance of local peak for peak alignment. The new alignment not only reduces computational overhead, but

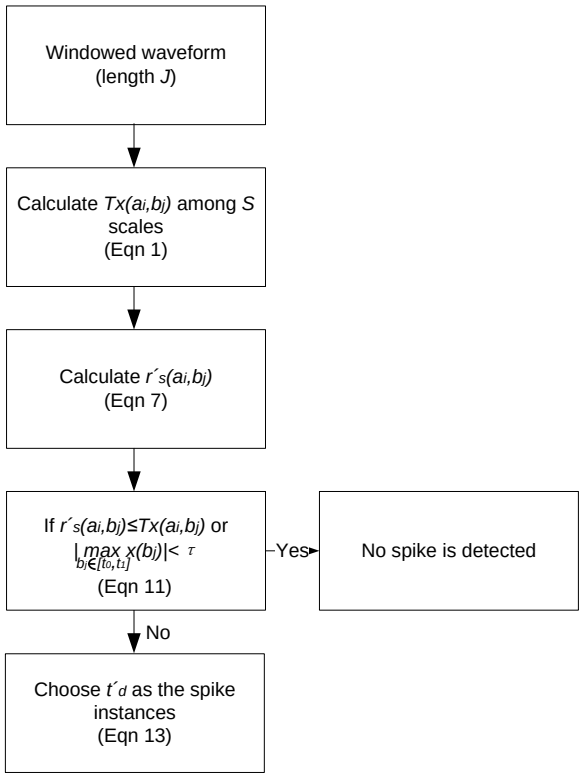

Figure 2.2: Flow graph of the revised MCWC

also improves classification accuracy. The flow graph of the revised MCWC algorithm is shown in Figure 2.2.

2.2.2 Template Generation and Spike Detection

The first step in using the proposed M-Sorter is to create spike templates using the MCWC algorithm introduced in 2.1 with a high S value in (2.4). By doing so only high quality spike waveforms with high amplitudes and clear temporal characteristics such as sharp rising and falling edges are identified by MCWC and therefore they can be used as spike templates. Only a small segment of the recorded neural waveforms is needed for template generation. For example, if original waveforms are collected at $24kHz$ for an hour, the first 1 minute data will suffice for template generation.

Let $Z = \{z^1, z^2, \cdots, z^p\}$ be the set of p detected potential spikes with a high S value, with S defined in (2.4). They are then classified using K-means to create the k potential spike templates. K-means clustering aims to partition Z into k sets ($k \leq p$), $Y = \{Y_1, Y_2, \cdots, Y_k\}$, so as to minimize the within-cluster sum of squares (WCSS):

$$\arg\min_{Y} \sum_{i}^{k} \sum_{z^j \in Y_i} ||z^j - m^i||_2, \tag{2.14}$$

where $\{m^1, \cdots, m^k\}$ are the respective cluster centers of $\{Y_1, Y_2, \cdots, Y_k\}$.

Manual aggregation of clusters to optimize the templates can be performed here. Given k_t ($k_t \leq k$) as the final cluster number based on human selection, $Y' = \{Y'_1, \cdots, Y'_{k_t}\}$ are the aggregated spike clusters with their respective centers at $\mu^i = \{\mu^1, \cdots, \mu^{k_t}\}$. Finally, μ^i is regarded as the ith spike template.

Note that, even though a high S value is used in the above procedure for template generation, but for actual spike detection, a low S value in (2.4) should be used. As discussed in [1], a low S value corresponds with a relatively low threshold when MCWC is viewed as an automatic and adaptive thresholding algorithm (Figure 4 in [1]). The MCWC with a low S value selectively identifies potential spike waveforms with their shape resemblance to real spikes. This step eliminates a large number of waveform segments with high magnitude that may have been considered potential spikes by simple thresholding methods. Once going through the detection step using the original MCWC [1], by applying a new threshold τ in the revised spike detection hypothesis in (2.11) and (2.12), the potential waveforms selected by MCWC will be inspected and those with magnitude near noise level will be removed from the pool of candidate spikes. As such, the revised MCWC detection can generate a high quality pool of potential spike waveforms with good spike characteristics and magnitude higher than the noise floor.

2.2.3 Template Matching

After spike detection, template matching is performed. Let $U = \{u^1, \cdots, u^j, \cdots, u^n\}$ be the detected potential spikes with a low S value. Simple correlation coefficient and Euclidean distance are used here to measure similarity between the templates and potential spike waveforms. Let N be the number of samples in a template spike waveform, denote $\mu^i = [\mu_1^i, \cdots, \mu_N^i]^T$. Let $\bar{\mu}^i$ and σ_{μ^i} be the sample mean and standard deviation of μ^i, respectively. By the same token, I define $\bar{u}^j$ and σ_{u^j} similarly. The correlation coefficient between each potential spike u^j and template μ^i is defined as

$$\rho_{ij} = \frac{E[(\mu^i - \bar{\mu}^i \times e)^T (u^j - \bar{u}^j \times e)]}{\sigma_{\mu^i} \sigma_{u^j}}, \tag{2.15}$$

where e is an N-dimension column vector of all 1's. And the Euclidean distance d_{ij} is

$$d_{ij} = ||u^j - \mu^i||_2. \tag{2.16}$$

For template matching, if the two criteria using the two measures ρ_{ij} and d_{ij} are met, i.e., $\rho_{ij} > \rho_0$ and $d_{ij} < d_0$, then the potential spike u^j is assigned to the ith spike cluster according to (2.17),

$$i = \arg\min_i d_{ij}. \tag{2.17}$$

Overall, the M-Sorter, as shown in Figure 2.1, is designed for automatic processing of spike detection and sorting based on the extracted templates. The first step of template generation aims at extracting spike templates with good spike features. Human supervision can be performed here to help choose the templates. The second step of detection using the revised MCWC detects the possible spike waveforms with magnitude larger than noise floor level. Based on the pool of well-shaped po-

tential spikes, simple measures of similarity are utilized in the third step of template matching.

2.2.4 Design Parameters

The M-Sorter is facilitated with three design parameters that are critical for the performance. These parameters include the scale value S in (2.4), the threshold τ in (2.11) or (2.12), and the cluster number k in (2.14).

S and τ are the two parameters reflecting the noise levels of the recorded waveforms. In the template generation step, a high S value should be chosen to produce high quality spikes; while in the detection step, a low S should be used. The threshold value τ, unlike in most thresholding based methods, is not crucial, and a relatively small value around the root mean square value of the background noise will suffice since it is used as a supplementary step to the MCWC. As for k, as shown in [3], hierarchical clustering idea can be exploited. Practically, a large cluster number is preferable if no prior information is available, and then aggregating similar clusters can be done under human supervision during template generation. I will show the corresponding results about these parameters in details in the next section.

Two other parameters, ρ_0 and d_0, are needed in template matching. Since they both reflect on the similarity to a template while taking into consideration of background noise, the following choices are recommended: $\rho_0 \in [0.75, 0.85]$ and $\sqrt{d_0}$ is less than 10% of the spike magnitude, i.e., $d_0 < (10\% \times ||\mu^i||)^2$.

For Matlab implementation of the M-Sorter, some additional parameters related to the experimenter's recording equipment setting need to be specified. They include the recording system sampling frequency f, bandpass filter band f_{lo} and f_{hi}. The M-Sorter code is available at `https://sites.google.com/site/jenniesisite/Home/software`.

2.3 Test Data Description

Seven data sets from four different sources are used to demonstrate the use of the M-Sorter and its efficiency. Comparisons with the Offline Sorter and the Wave Clus [4] are provided. Three artificial data sets (A, B and C) were used by Wave Clus [4] at two different noise levels. Two additional artificial data sets (D and E) were from the Noisy Spike Generator [28] at six different noise levels. Data set F, which contains 4 subsets, was downloaded from the Plexon website (`http://www.plexon.com/downloads.html$\#$Software`). Since no truth data was provided in association with the waveforms, data set F was considered for real neural recordings. Finally, data set G was captured from two rats' motor cortical areas while the rats were freely moving around.

Data sets A, B and C were from Wave Clus [4]. Each of the three data sets was 60 second long with three clusters. The waveforms in the three data sets were constructed based on neural recordings in the neocortex and basal ganglia where manually extracted spikes were contaminated by artificially adding different levels of noise. Two levels of noise with standard deviations equal to 0.05 and 0.2 of the original waveform were used in the data. Among the three data sets, data set A was considered easy to sort while data sets B and C were difficult.

Data sets D and E were created using Noisy Spike Generator [28] under its default setting with SNRs equal to $25, 15, 13, 12, 11$ and 10. Each subset was 60 second long, and sampled at $24kHz$. Data set D had 3 clusters, and E had 2 clusters. The spike waveform magnitudes were normalized to 1.

Data set F was obtained from Plexon website where the sampling frequency was $44.1kHz$. Since no truth was provided, it was considered a real neural recording.

Data set G contained 2 subsets of real neural recordings via tungsten microarrays implanted in the rats' motor cortical areas. Rats were moving freely when the recordings were taken. Each subset in G was 20 second long. The neural waveforms were sampled at $24.414kHz$.

All the signals were digitized, and bandpass filtered between $300Hz$ and $3kHz$ using 3rd order butter-worth filter implemented in Matlab to eliminate low frequency drift and high frequency noise.

2.4 Measures for Sorter Performance

For artificial datasets, I used the total error and total accuracy as our figures of merit for each cluster of sorted spikes. The error and accuracy are defined as

$$T_{err} = 100 \times \frac{N_{FP} + N_{FN}}{N_{TP} + N_{FN}}, \tag{2.18}$$

$$T_{acc} = 100 \times \frac{N_{TP}}{N_{TP} + N_{FN}}, \tag{2.19}$$

where N_{FP} is the number of false positives, N_{FN} is the number of false negatives, and N_{TP} is the number of true positives. A true positive spike is one that was detected within an acceptance interval of $\pm 0.5ms$ from the truth and was also correctly clustered according to the truth. If a spike was announced without presence of a truth, it was then counted as a false positive. If no spike was announced while there was one according to the truth, then it was counted as a false negative.

However, these performance measures are not appropriate for applications to real neural recordings since no true spike times and cluster information were available. Thus, for real recordings, features such as spike duration, template reconstruction,

spike shape, and intra cluster distance are investigated as indicators of spike sorting performance.

To gain perspective on how the M-Sorter compares with other popular sorters, I compared M-Sorter performance to two thresholding based systems: the Wave Clus [4] and the Offline Sorter (Plexon Inc). For comparison purposes, for each data set, I used different S values for the M-Sorter, different threshold values for the Offline Sorter to minimize the total error while maximizing the total accuracy. The Wave Clus algorithm automatically selects its threshold values.

2.5 Impact of the Free Parameters on the M-Sorter Performance

In this section I provide evaluations of the key parameters in the M-Sorter and their impact on M-Sorter performance.

Data set C-2 (noise level 0.05) is used herein to demonstrate the impact of free parameter selection on M-Sorter performance. The goal here is to test the M-Sorter performance in the detection stage at different parameter settings. The following set of parameters were used: $S = \{2, 3, \cdots, 8\}$ in (2.4) and thresholds $\tau = \{0, 15, 20, 25, 30\}\mu V$ in (2.11) and (2.12). The corresponding correct detection and false alarms are summarized using the ROC curves as shown in Figure 2.3.

In Figure 2.3a, the results of different thresholds are displayed. When $\tau = 0$ (corresponds to the original MCWC algorithm, the line with the stars), it detected the most true spikes (the top point on the starred line, when $S = 2$, $T_{acc} = 97\%$) with the most incorrectly detected spikes ($T_{err} = 95\%$). As the threshold increased, the ROC curves moved to the left. For example, by applying a threshold of $\tau = 15\mu V$ (the solid line with triangles), the error rate reduced to $T_{err} = 37\%$ (when $S = 2$), while the correct rate remained ($T_{acc} = 94\%$). As the threshold increased from $\tau = 0$ to $\tau = 30\mu V$, the error rates decreased, however, the true positive rates also decreased.

A trade-off is thus necessary to select a good pair of S and τ. When the threshold increased to an extremely high value, for example, $30\mu V$ (the dotted line with circles), the error rate reached a small value ($T_{err} = 0.4\%$); on the other hand, the correct rate fell down to $T_{acc} = 86\%$. Thus, the application of a threshold can remove part of the noise if it is set appropriately, but too high a threshold will greatly reduce the correct detection rate.

The false alarm rates for different combinations of S levels with τ values are shown in Figure 2.3b. Without thresholding by τ, the rightmost points of each curve indicate the largest false alarm rates within each S level. As the S value increased, the error rates decreased, but the correct detection rates also decreased dramatically. By combining MCWC with the threshold τ, the detection results became more robust (e.g., when $S = 2$, the correct detection rates remain higher above the results for $S = \{3, \cdots, 8\}$, while the error rates decreased as τ was integrated). Therefore from Figure 3, it is not difficult to see that a low S value (e.g., $S = 2$) plus a reasonable threshold τ (e.g., τ set at the noise floor level) usually provides the most desirable performance - high detection rate with low false alarms.

The false alarm rates for different S levels and threshold value combinations are shown in Figure 2.4. It is clear that thresholding helped reduce noise most effectively under small S values.

2.6 Comparisons of Sorters

In this section, I provide a comprehensive comparison among the three systems (the M-Sorter, the Offline Sorter and the Wave Clus) on the seven data sets.

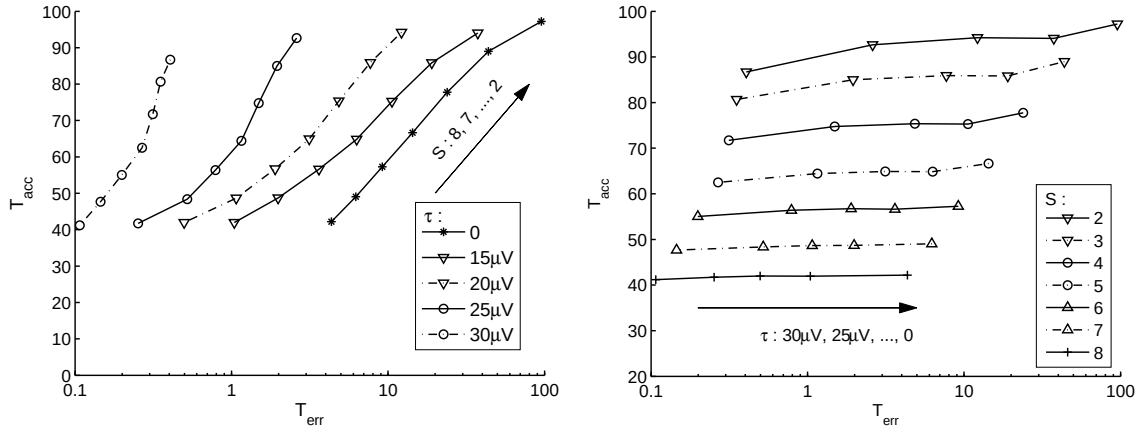

(a) ROC curves for different τ values

(b) ROC curves for different S levels

Figure 2.3: ROC curves of MCWC-based detection results. Note that $\tau = 0$ is the case of the original MCWC [1].

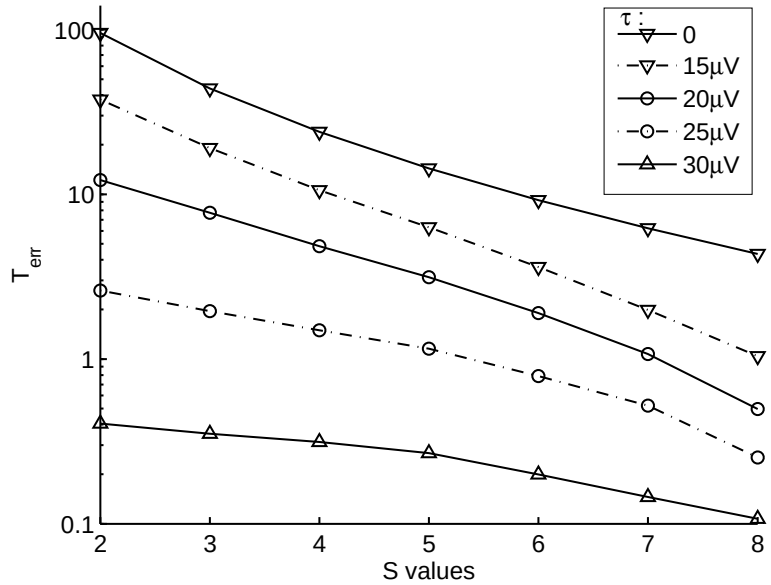

Figure 2.4: False alarm rates for different combinations of S values and threshold τ values

2.6.1 The Offline Sorter and the Wave Clus

The Wave Clus has its own selection of threshold value τ_W, which has three possible modes in detection: positive, negative and both, for a threshold crossing from below, crossing from above, or either case, respectively.

$$\tau_W = 4\delta_n, \tag{2.20}$$

where

$$\delta_n = median\{\frac{|x|}{0.6745}\}. \tag{2.21}$$

The Offline Sorter also provides several different thresholding methods including, for example, raw signal and variations on energy of the signal. The energy E of a signal is defined as

$$E(i) = \frac{1}{W}\sum_{j=i-W/2}^{i+W/2} v^2(j), \tag{2.22}$$

where $v(i)$ is the raw signal at time i, and W is the window width. In the dissertation, $W = 3$ was used if the method Energy was chosen. In our comparison, I explored different threshold values to reach a good compromise between accuracy and error.

The Offline Sorter is facilitated with several sorting methods including, for example, T Distribution and Valley Seeking. Different methods usually produced different results and spike clusters, and I manually chose the best result closest to the truth, or the most reasonable result by human inspection. Since I used the T Distribution option of the Offline Sorter, whenever Offline Sorter is used in this dissertation, it refers to this specific mode.

When using the M-Sorter, a relatively low threshold was set as discussed in the previous section. Different S values were tested, and the best results were chosen and analysed.

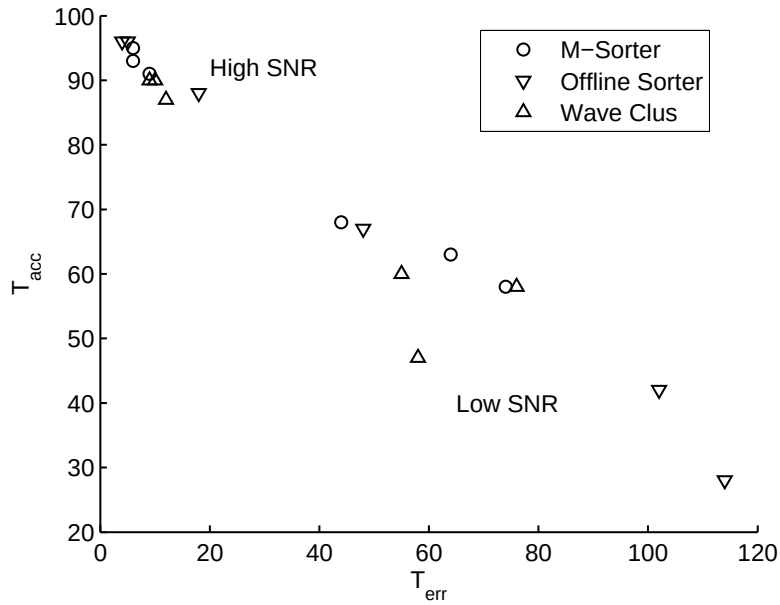

Figure 2.5: Results of data sets A-C

2.6.2 Comparing Sorters using Artificial Data Sets A-C

For artificial data sets A-C, the results are displayed in Figure 2.5. For high SNRs, all three methods performed equally well, with low error rates ($T_{err} < 20\%$) and high accuracies ($T_{acc} > 85\%$). However, when more noises were added to the signals, the overall performance of the three methods degraded. Data set A was an easy case, and the three methods were equivalent in performance, with accuracies around 60% and error rates around 50%. For data sets B and C, the M-Sorter and the Wave Clus were competitive with accuracies of 60% and error rates of 60%, while the Offline Sorter was unable to discriminate between two very similar clusters, and therefore producing low accuracy and high error rates.

For artificial data sets D and E, the results based on different SNRs were displayed in Figure 2.6. Due to its automatic estimation of thresholds, the Wave Clus either missed a large percent of true spikes, or resulted in significant false alarms. Overall,

I again found that all algorithms performed remarkably well for high SNRs, where the error rates were around 50% for data set D, and 15% for data set E, and the accuracies were around 65% for data set D and 90% for data set E. Performance differences were more pronounced for the more difficult cases with low SNRs, with the error rates going up and accuracies going down.

While all algorithms showed a drop in performance as SNR decreased, the M-Sorter and the Offline Sorter were competitive, with the former identified the largest number of correct spikes and produced the least error. As shown in Figure 2.6a, both produced accuracies around 90% and error rates around 20% when SNRs were high. For $SNR = 13$ or lower, the M-Sorter showed its robustness in differentiating between clusters. Although both systems had similar accuracies, the M-Sorter showed smaller error rates than the Offline Sorter. In Figure 2.6b, they had competitive performance for $SNR > 12$. As SNR went below 12, the M-Sorter showed a little advantage. In summary, the M-Sorter was comparable to the Offline Sorter for high SNRs, and it offered a little better performance than the Offline Sorter for low SNRs.

2.6.3 Comparing Sorters using Real Data by Plexon

For each of the four data sets in F provided by Plexon, no truth was available. Thus, they were considered as real data. Spike clustering results were compared. For the Offline Sorter, I lowered the threshold, to include as many potential spikes as possible, and the threshold was set to 0.25. And Valley Seeking sorting program was used. For M-Sorter program, $S = 2$ and a low threshold $\tau = 0.2$ was used for all four data sets in F.

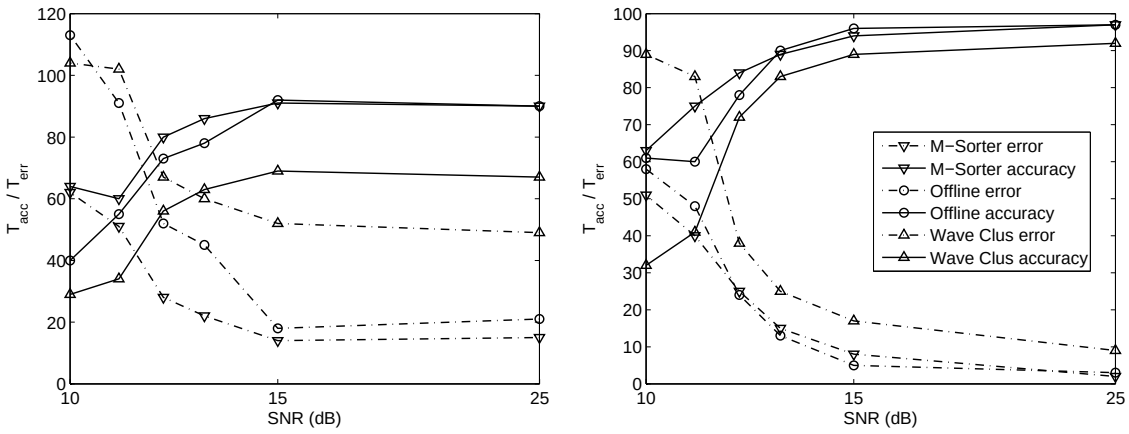

(a) Results for data set D

(b) Results for data set E

Figure 2.6: Performance comparison of artificial data sets D and E, where the solid lines are for accuracy while the dashed line are for error rates.

The spike sorting results of the M-Sorter and the Offline Sorter are shown in Figure 2.7, together with the averaged intra-cluster variance, which is defined as

$$v = \frac{1}{n_i} \sum_{j=1}^{n_i} \left(u^j - \mu^i\right)^2, \tag{2.23}$$

where u^j is the jth spike in cluster i, μ^i is the ith cluster center and n_i is the total number of spikes in cluster i.

For data set F-1, both sorters generated similar spike numbers. The Offline Sorter had five clusters, where cluster 2 and 4 look similar. For the other data sets, the Offline Sorter also detected more spikes than the M-Sorter in the total number for data sets F-2 to F-4. For data set F-2, the Offline Sorter and the M-Sorter were similar in cluster 3 and 4, but the Offline Sorter generated higher spike numbers in cluster 1 and 2. For F-4, the 1st cluster of the Offline Sorter had 47% spikes more than the M-Sorter. Through the four data sets, the Offline Sorter and the M-Sorter performed equally when comparing the variances. As an example, I provide the resulted waveforms for F-4 in Figure 2.8.

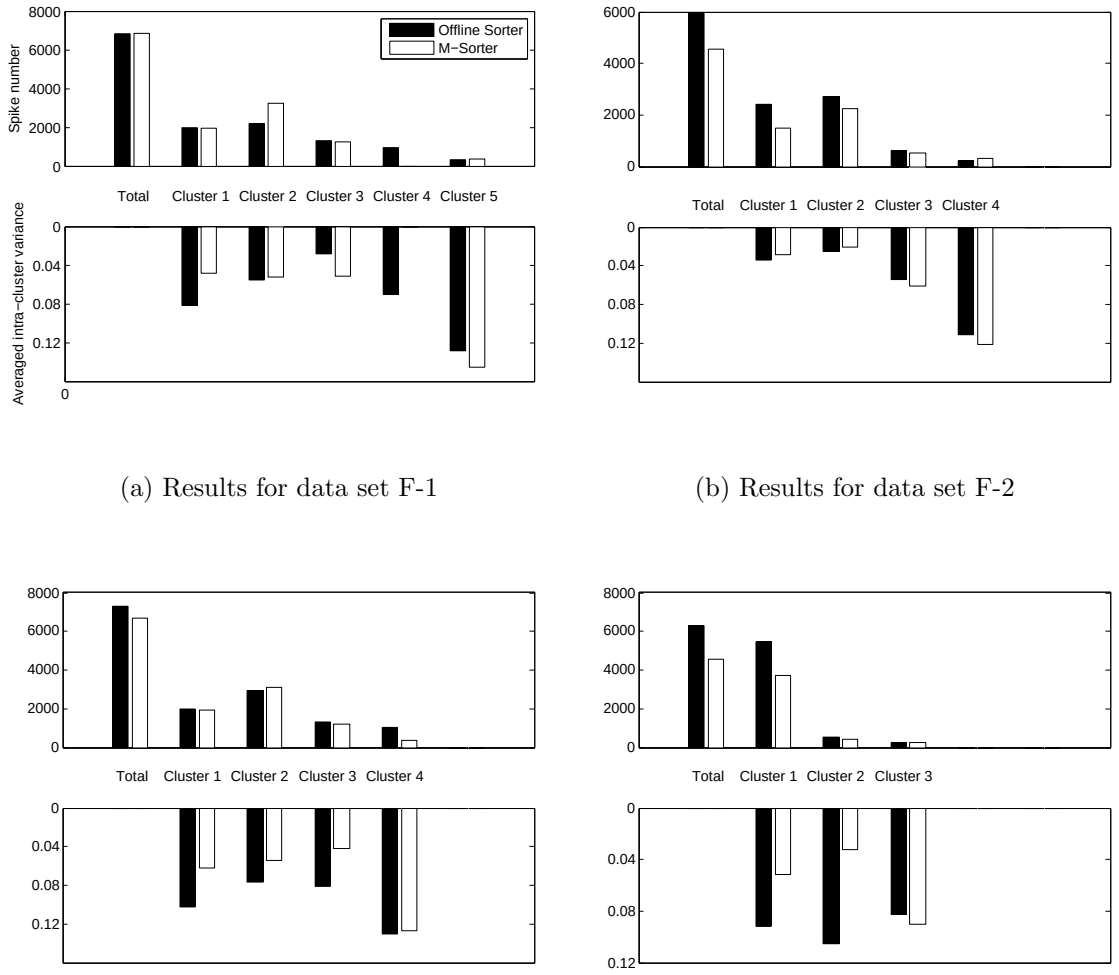

(a) Results for data set F-1

(b) Results for data set F-2

(c) Results for data set F-3

(d) Results for data set F-4

Figure 2.7: Detection and sorting results for data sets F-1 to F-4 using the Offline Sorter and the M-Sorter.

The averaged (grey curves) and sorted spike (black curves) waveforms are shown in Figure 2.8. The M-Sorter and the Offline Sorter both generated three clusters. For all the clusters, the spike duration were about 1ms. Cluster 1's amplitude was about 0.2, while the other 2 clusters were around 0.5. The spike numbers in cluster 2 and 3 were close. However, the spike numbers differed significantly for cluster 1. By inspection, the Offline Sorter had a few false alarms, and the resulted waveforms had a larger variance compared with the M-Sorter. This result agrees with those obtained by investigating the artificial data sets previously that thresholding introduces significant false alarms. By only using the waveform amplitude, other important features of a spike were ignored.

2.6.4 Comparing Sorters using Rats' Motor Cortical Data

I performed similar computations and comparisons for the 2 sets of real data G-1 and G-2, as did in the previous subsection for data sets F-1 to F-4. For the 2 sets of real data, I ran the Wave Clus automatically, and selected the threshold carefully for the Offline Sorter and the M-Sorter. By investigating the results briefly, the Wave Clus produced results that were significantly deviated from those by human inspection and was excluded in the following comparison.

For data set G-1, different threshold values were tested for the Offline Sorter, and finally it was set to $-35\ \mu V$. A total number of 716 spikes were detected and sorted to 2 clusters plus a noise cluster, while only the spike clusters are summarized and shown in Figure 2.9, and the noise cluster is not included. The M-Sorter detected 1860 spikes using $S = 2$ and threshold $-25\ \mu V$, among which 481 and 304 spikes were clustered. Similar variances in each cluster by each algorithm were observed.

For data set G-2, the Offline Sorter resulted in 1789 spikes and were sorted into 2 clusters (1200 and 549 spikes, respectively, Figure 2.9) plus a noise cluster (not

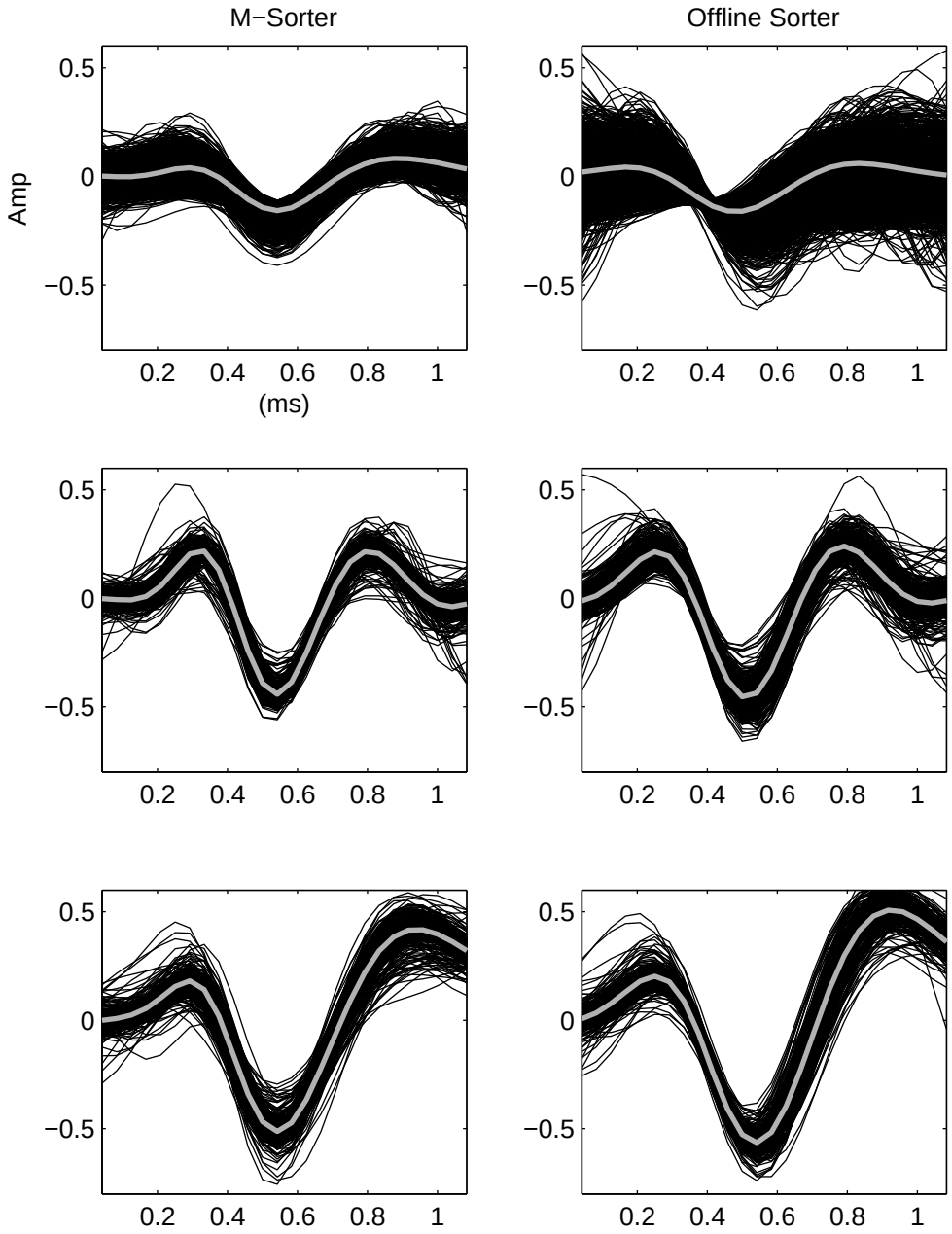

Figure 2.8: Waveforms of sorted spikes for artificial data set F-4. The grey waves are averaged results of respective spike clusters.

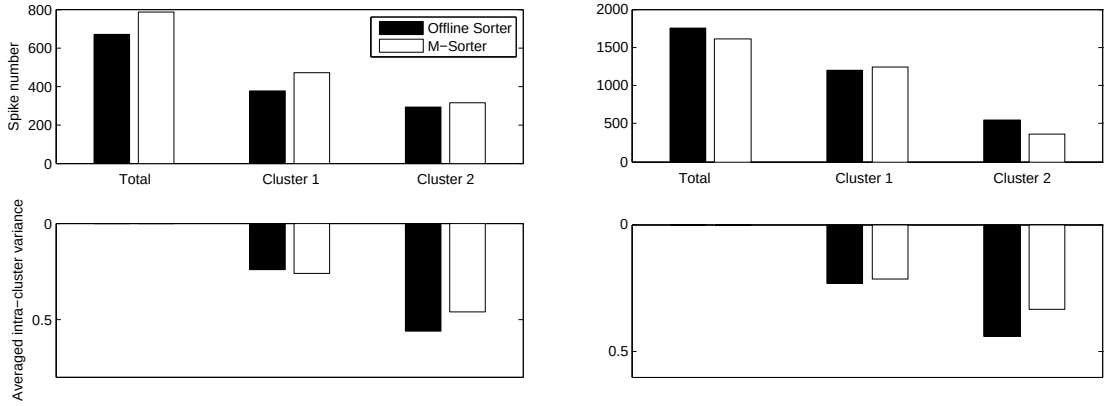

(a) Results for data set G-1

(b) Results for data set G-2

Figure 2.9: Detection and sorting results for data sets G-1 to G-2 using Offline Sorter and M-Sorter.

shown). The M-Sorter detected 2823 spikes, among which 1248 and 359 spikes were from 2 neurons. For both sorters, cluster 1 had similar variances. The waveforms were further studied and shown in Figure 2.10. The averaged waveforms (grey curves) were similar, while the Offline Sorter had a larger variance. To investigate the sorter performance in details, a period of the raw waveform and the sorted spikes are shown and marked in Figure 2.11.

By comparing the results, the M-Sorter and the Offline Sorter resulted in similar numbers of clusters and spikes, while the M-Sorter results appeared more resistant and less sensitive to parameter changes. These results agree with those using artificial data sets.

The results by the M-Sorter reported in this dissertation were all implemented and tested using Matlab R2009a (Mathworks, Natick, MA). The computer where the simulations were performed is equipped with an Intel Core (TM) 2 Quad CPU Q6600 2.40GHz with 3.50GB of RAM. As previously reported in [1], the MCWC algorithm

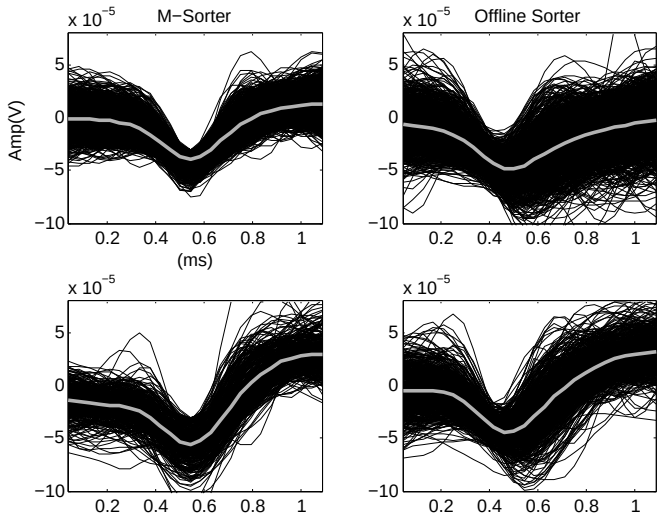

Figure 2.10: Sorted and averaged spike waveforms for real data set G-2.

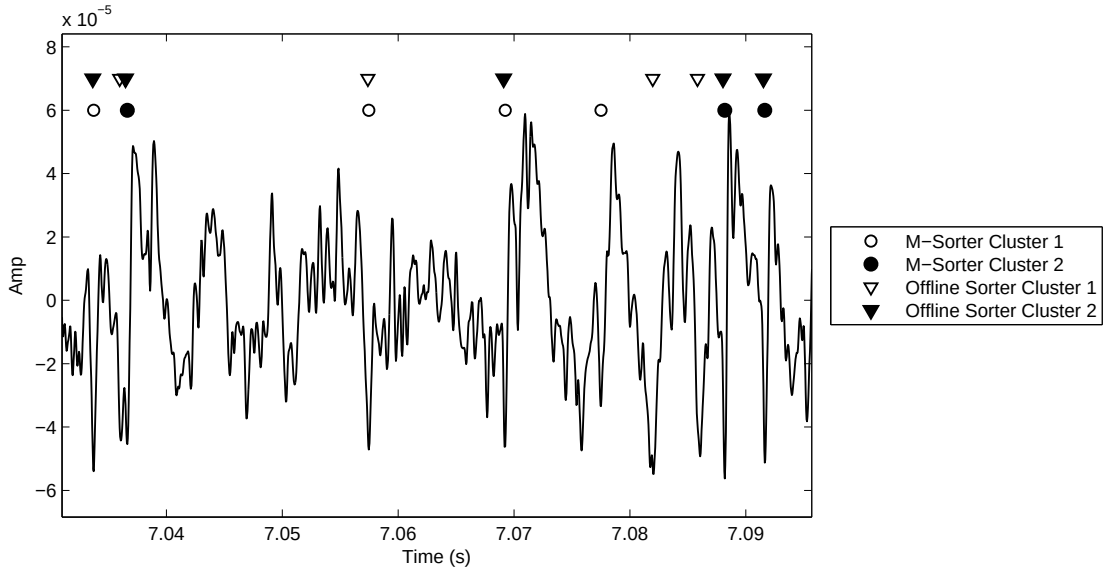

Figure 2.11: A randomly selected spike waves from data set G-2 with sorted spikes shown on top.

was potentially real-time implementable. The M-Sorter is also potentially realizable in real time. In-depth discussions on this issue will be provided elsewhere.

2.7 Conclusions

Given the powerful recording systems with the capability of simultaneously sampling from dozens to hundreds of neurons, there is an urgent need to develop and optimize methods to handle the massive amount of neural data. Reliable identification of neural spikes provides a great opportunity for important future discoveries in neuroscience. Our proposed M-Sorter is advantageous in the following aspects. First, due to a reliable detection step prior to classification, the M-Sorter has produced much less false alarms than the usual thresholding. Second, the extracted templates used by the M-Sorter for spike sorting are selected from the original neural waveforms with good quality and this is possible even when the quality of the waveforms are not ideal. Third, the M-Sorter is potentially real-time applicable. Finally, only a few parameters are up to the user's choice and they are easy to select. As shown, the M-Sorter is consistent in results, robust to parameter variations, and is especially advantageous to use under less than ideal waveform conditions.

Chapter 3

THE DIRECTIONAL CHOICE TASK

3.1 General

Male Long-Evans rats were cared for in accordance with the guidelines set forth by the Institutional Animal Care and Use Committee at Arizona State University. The animals weighed 50 g upon arrival into the laboratory. They were handled daily and started the pre-training stage of this experiment when they reached 300 g.

During this initial stage, the rats were placed in a Skinner box (Med Associate Inc., St Albans, VT) where two light-emitting diodes (LEDs), one on each side, were placed right above two extensible paddles. It is equally likely to have one of the two LEDs turned on as the start of a new trial. The control paddle on the same side under the LED would extend 2.0 s later. Pressing the control paddle within 30.0 s would turn off the LED and also lead to a 1 kHz reward tone and a sugar pellet reward. No action within the time allowance would automatically terminate the trial and lead to a punish tone of 12 kHz, no sugar pellet reward, and a 10.0 s timeout. The inter-trial interval was 5.0 s.

The rats used in this study were trained for a mean of 72 ($\pm$ 36, SD) sessions and reached 90% accuracy. At the end of this stage of the experiment, the rats were not only proficient with the association between an LED light cue and the paddle, but they also had become skilled at paddle pressing.

After the pre-training stage and when the animals reached 400 g, they were implanted with microwire arrays. Upon recovery, the animals were placed in another Skinner box (Med Associate Inc., St Albans, VT), and began learning the directional choice task described below, while single-unit neural signals and behavioral performance data were recorded simultaneously.

Twelve ($n = 12$) rats (A, B, C, D, E, F, G, H, I, J, K, and L) were used for study in Chapter 4. Within the 12 rats, 6 rats (Rats C, D, E, F, G, and H) were used in behavioral and electrophysiological recordings; 4 rats (Rats I, J, K, and L) were used in video recording; 2 rats (Rats A and B) were used in both behavioral and electrophysiological recordings and video recording.

Ten ($n = 10$) rats (A, B, C, D, E, F, G, H, M, and N) were used for study in Chapter 5. All the 10 rats provided behavioral and electrophysiological recordings.

3.2 Surgery

The surgical procedure was performed using aseptic techniques. Each rat was anesthetized by injection of the KXA mixture (10.0 mg/ml ketamine, 2.0 mg/ml xylazine, and 0.1 mg/ml acepromazine; 0.1cc/100g, administered intramuscularly). Heart rate and O2 saturation were continuously monitored. Once into an anesthetized state, each rat was placed in a stereotaxic frame with ear bars inserted and front teeth latched. The surgical area was then draped. Skin and fascia were removed to expose bregma plus sufficient area for performing the craniotomy and placing anchoring screws. A craniotomy of approximately 2mm×4mm centered at 2.0 mm lateral and 3.0 mm rostral from bregma was removed. This allowed the insertion of the microwire array. The 16-channel (2×8) microwire array (Tucker Davis Technology or TDT, Alachua, FL) was then lowered into the left hemisphere of each rats brain. The tips of the microwire array were cut at 60 degrees. The electrode row spacing was 500 μm (rats A, B and H) or 375 m (rats C, D, E, F and G). The electrode column spacing was 500 μm. An acrylic head cap was fixed on the skull with three anchoring bone screws. Sutures were used, if needed. Two supplemental doses of KXA (0.05 cc/100g) were provided with approximately one hour separation during the procedure. A KX (20 mg/ml of ketamine and 3 mg/ml of xylazine in 0.9% NaCl solution) update (0.05

cc/100g) was applied if needed after the two KXA supplements. Systemic antibiotics and analgesics were administered for three days after the surgery.

3.3 Directional choice task

Upon recovery from the implant surgery, rats began a series of sessions in which they learned the directional choice task. As they did so, we recorded single-unit neural activity and behavioral data simultaneously. One experimental session of about an hour was conducted per rat each day. Throughout the experiments, the rat was free to move about inside the Skinner box.

Five LEDs were located on the front panel of the box as shown in Figure 3.1C: one in the center, two on each side. Hereafter, when I refer to a "light" I identify one LED that was illuminated while the others were not. There were three paddles that the rat could press, one to the left, one in the center, and one to the right. The left and right paddles were located lower than the center paddle, as illustrated in Figure 3.1C.

In order to obtain a sugar-pellet reward, the rat needed to press either the left or right paddle to control the location of the illuminated light, which varied among the five possible positions. The rat began each trial by pressing on the central paddle. Later, a left-paddle press would shift the light to the right by one position and a right-paddle press would shift the light to the left by one position. Thus, the correct response was to press the paddle on the side of a light in order to shift it toward or to the central position. No response was required to the center light.

Each trial proceeded as follows: as soon as the center paddle was depressed by the rat, one of the five cue lights, chosen at random, was illuminated immediately. I called this event "cue onset". Both the left and right control paddles extended into the testing box 2.0 s later. The rat was allowed 1.0 s to complete a first paddle press,

and another 4.0 s for a second paddle press if the cue light required two presses to illuminate the center light. A trial would be terminated in any of the following three conditions: (1) if the cue light was moved to the center by making the correct control presses and the light remained in the center position for at least 1.0 s. In this case the trial ended as a success. As a special case, trials with the center cues were successfully ended if the rat did not press any paddle within 1.0 second; (2) if the cue light did not reach the center location within the time allowance then the trial ended as a failure; and (3) if the light was moved outside of the cue light area (i.e., farther to the left when at the extreme left position or farther to the right when at the extreme right position) then the trial was also considered a failure.

All successful trials were associated with an immediate low-frequency reward tone of 1 kHz along with a sugar pellet reward 0.5 s later. Failed trials were associated with a high-frequency tone of 12 kHz without any reward. The rat could start a new trial after an inter-trial interval of 8 s for successful trials and 15 s for failed trials. An example of a task sequence is given in Figure 3.1C. The trial cues were presented randomly in blocks of 25 trials and the performance accuracy in response to each cue was calculated for each block. After each block of 25 trials, the next 25 cues were programmed in a way that a slightly larger number of cues would be those that had resulted in a greater frequency of failed trials during the previous session.

3.4 Video acquisition

I captured image sequences with a spatial resolution of 0.47 mm/pixel at 25 frames per second when the rats were performing the directional choice task. A video camera was mounted at the back of the Skinner box facing the front control panel. Infrared LEDs were placed inside the Skinner box as house light. Camera focus was tuned

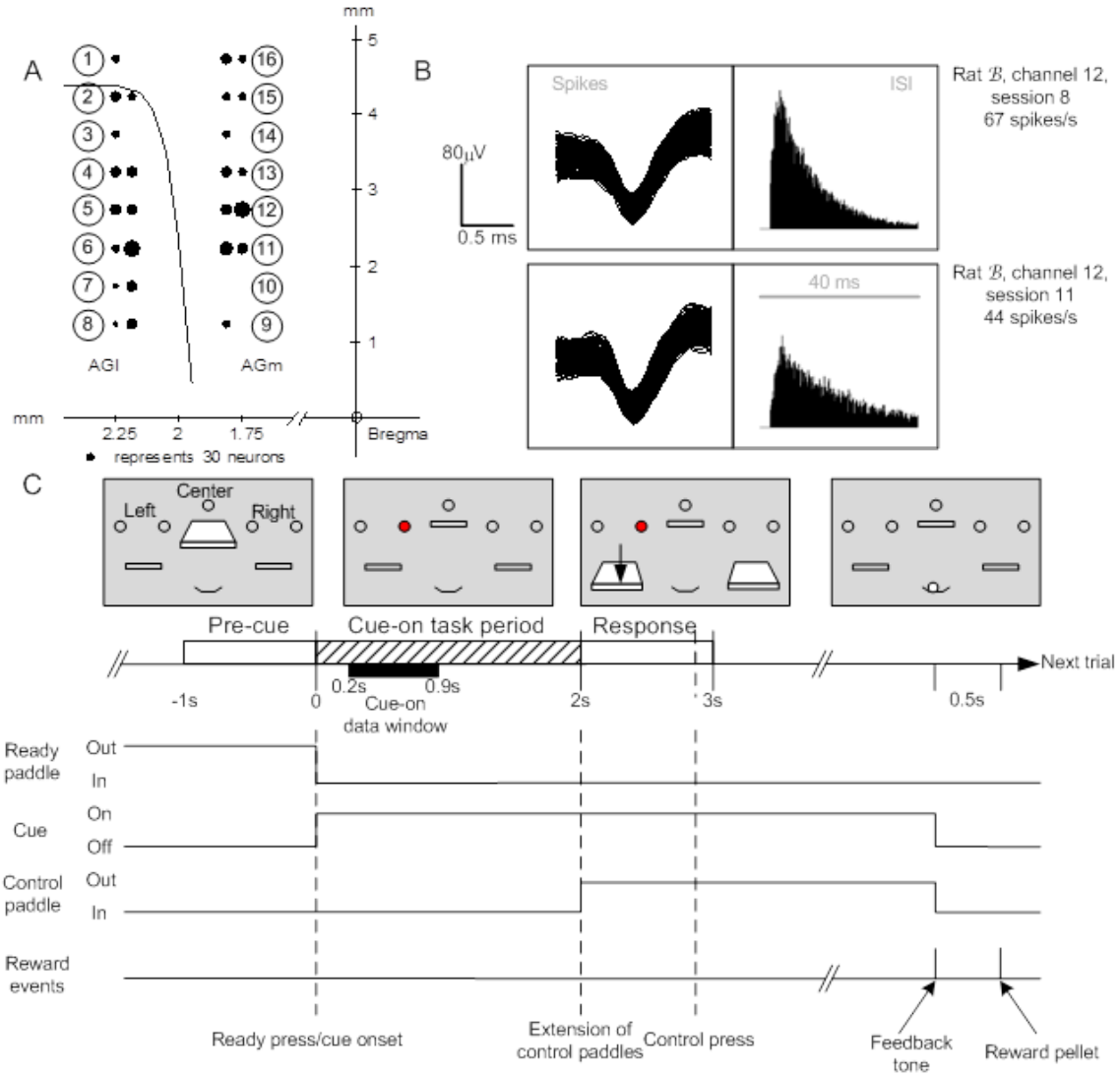

Figure 3.1: Implant site and illustration of the behavioral task. A, implant site and hit map of the recorded units. A 16-channel (2×) microwire array with electrode numbers labeled was implanted in the rat's left hemisphere centered at 3 mm AP, 2 mm ML from the bregma. The delineation of AGm and AGl was made according to the Rat Brain Atlas (Paxinos and Watson, 2005). The hit map is a summary of all units from the 8 implanted rats. B, example spike waveforms and ISI histograms in 2 different sessions. C, the behavioral control panel facing the rat and task trial timelines. Three task periods were defined. The pre-cue task period lasted 1 second. A 2.0-s cue-on task period followed immediately. The cue-on data window was 0.2 to 0.9 s after the cue onset. The response task period started from the instance of the extension of side control paddles and lasted for 1.0 s.

manually when needed prior to starting a new recording session. The rat's head and body positions were clearly visible on most frames.

3.5 Video analysis

For each video frame, I extracted three pairs of variables: the implant head cap position (h_x, h_y), the left ear position (l_x, l_y) and the right ear position (r_x, r_y). The rat head position for this frame is then calculated as the means of the three pairs of variables: $(H_x, H_y) = ((h_x + l_x + r_x)/3, (h_y + l_y + r_y)/3)$. Each trial usually consisted of 59±5 frames, which amounted to 2.32±0.20 s from the trial cue onset through the time when the rat made the response press. A sequence of rat's head positions were obtained accordingly. The exaction of these variables from the image sequences was performed in a semi-automatic fashion with part of the procedures performed by custom Matlab code (Mathworks, Natick, MA).

3.6 Analysis of trajectories, movement starting and ending time

After the head positions $(H_x, H_y)$for each trial, I calculated the rat's movement speed at the ith frame as $s_i = \sqrt{(H_x^{i+1} - H_x^i)^2 + (H_y^{i+1} - H_y^i)^2}/40(pixel/ms)$. Let the movement threshold parameter $t = 0.5 \times \sqrt{(1/n(s_1^2 + s_2^2 + \cdots + s_n^2))}$, where n is the number of frames in the trial. The movement start time S was considered as the time when the rat's speed rose above the threshold and remained so for 5 consecutive frames while the movement end time E was considered as when the rat's speed fell below the threshold and remained so for 5 consecutive frames. By the end time E, the control paddle was usually within reach by rats. The movement duration was thus obtained as $D = E - S$. Corresponding to the start time, the movement start position was the head position where the rat started to move. Similarly, the movement end position was the rat's head position at the end time.

3.7 Recording session and spike sorting

Multi-channel chronic single unit recordings from the rat's AGm and AGl areas were obtained using either the RX5 Pentusa Base Station or the RX7 Microstimulator Base Station (Tucker Davis Technology or TDT, Alachua, FL). Original neural waveforms were digitized at 24.414 kHz and saved. Spike sorting and other processing of the raw waveforms took place offline. The neural signals usually maintained strong spike presence for approximately 20 30 recording sessions post surgery. All behavioral event markers were recorded simultaneously with the neural signals.

The stored waveforms were extracted from TDT data tank and bandpass filtered between 300 Hz-3 kHz. Offline spike detection and sorting was performed using the M-Sorter from our own lab [57]. The sorter utilizes the multiscale correlation of wavelet coefficients (MCWC) for spike detection [1].Then the k-Means clustering and template matching algorithms were used to classify single units. The M-Sorter has been tested extensively using artificial data sets and real neural recordings. Testing results by the M-Sorter were comparable with or better than the automatic mode (T-Distrubution E-M) of the Offline Sorter (Plexon Inc, Dallas, TX) and the Wave_clus algorithm [4]. The sorted spikes were further inspected by the authors to ensure accuracy. The isolated putative single units were thus obtained. The spikes so obtained from each unit were consistent in waveform shape, formed separable clusters in PCA space from other neurons in inter-spike interval (ISI) histograms. The spike width was usually larger than 0.5 ms. Isolated units and the time stamps of spiking events along with behavioral event markers were then stored for the analyses performed in this study. Figure 3.1B shows example neural spike waveforms and their respective ISI histograms.

3.8 Stimulation

To verify the recording sites, intracortical microstimulation was applied using the RX7 Microstimulator Base Station and MS16 Stimulus Isolator by TDT. Passive headstage was used in the procedure. Two rats, J and K, were stimulated after their behavioral and neural data recording using the same implanted electrodes as those for recording neural activities. The animals were lightly anesthetized using KX during stimulation when a train of 13 cathodal pulses was presented at 312.5 Hz. Each pulse was 0.2 ms in duration. Stimulation always started using a small current of 20 μA, and increased up to 60 μA in most cases. In one case (rat J) the stimulation current was increased to 100 μA. For rat J, electrodes 5-8 (Fig. 3.1A) elicited contralateral whisker movements at 60 μA current. When the current was increased to 100 μA, electrode 6 elicited right forelimb movements and whisker movement. For rat K, electrodes 7 and 8 elicited contralateral whisker movements and neck movement at 60 μA current.

3.9 Performance accuracy measures

I calculated each rats performance accuracy, R, in each session. R was the ratio between the number of successful trials N_s and the total number of trials N during the session, expressed as percent correct, i.e., $R = N_s/N \times 100\%$. Also, I let N_e denote the number of failed trials. Post-error accuracy R_{es} was the ratio between the number of successful trials immediately after a failed trial N_{es} and N_e, also expressed as percent correct, i.e., $R_es = N_{es}/N_e \times 100\%$. Likewise, the post-success accuracy R_{ss} was based on the ratio between the number of successful trials immediately succeeding a successful trial N_{ss} and N_s, i.e., $R_{ss} = N_{ss}/N_s \times 100\%$. These two measures together

with performance accuracy R were indicators of a rats ability to learn the task; the larger the R_{es} and R_{ss} values, the higher the performance accuracy.

3.10 Task-related neurons

The following three task periods were identified based on the behavioral task protocol (Figure 3.1C): pre-cue (1s before cue onset to cue onset), cue-on (from cue onset to 2s after), and response (from control paddle extension to 1s after). I considered a neuron task-related if, during at least one of the above defined three task periods, its trial averaged firing rate was significantly different from any of the other two task periods (Mann-Whitney U test, $p < 0.01$), where the firing rates were calculated as spike counts in 20-ms bins averaged over all trials during a session. The neural results presented in this report were based on all trials that the rat responded with a paddle press (left or right) with either successful or failed outcomes.

3.11 Neural modulation

To study neural modulations by previous trial outcome (success or failure) within the cue-on task period, I compared trial averaged firing rates using 20-ms bins for each task-related neuron. First, for each trial, a neuron's firing rate in the cue-on task period was represented by a 1×100 vector (2.0 s of data). Let Let $f_E(1)$ denote a neuron's firing rate vector averaged over all trials succeeding a previously failed trial. Also, let $f_S(1)$ be a neuron's average firing rate vector of all trials succeeding a previously successful trial.

To study the firing rate difference between post-error trials and post-success trials, I define the previous trial modulation measure I_1 as:

$$I_1 = \frac{f_E(1) - f_S(1)}{\max(f_E(1), f_S(1))}, \tag{3.1}$$

where $\max(f_E(1), f_S(1))$ denotes the largest element among $f_E(1)$ and $f_S(1)$, and $I_1 = (I_1^1, I_1^2, \cdots, I_1^i, \cdots, I_1^100) \in R^100$ with i denoting the time bins of the cue-on task period (2.0 s) within a trial. In addition, for $i = 11, 12, \cdots, 45$ it corresponds with the cue-on data window. The measure I_1 is an indicator of a neuron's firing rate difference in the three task periods in relation to previous trial outcome, respectively. The range for the measure is from -1 to 1. If $I_1^i < 0$, it means that the firing rates of post-error trials were lower than the post-success trials at the ith time bin. Conversely, if $I_1^i > 0$, it means that the firing rates of post-error trials were higher than the post-success trials at the ith time bin. In addition, the closer it is to +1 or 1, the more significant differences exist in the compared firing rates.

Let $|I_1|$ be $|I_1| = (|{I_1}^1|, |{I_1}^2|, \cdots, |{I_1}^100|)$. For each neuron, let $\tau_1 = \arg\max |{I_1}^i|$,$i = 1, 2, \cdots, 100$, i.e., at time τ_1, the difference in firing rates between post-error and post-success trials was the largest among all time bins in a trial. Also, I define a scalar $\bar{I_1}$ represents the averaged $\bar{I_1} = sum_{i=11}^{45} I_1^i$ representing the averaged values of I_1^i over the cue-on data window.

3.12 Neural modulation measured by ROC and AUC

To analyze differences in distributions of neural responses between post-error and post-success trials, I used the receiver operating characteristics (ROC) [58]. The ROC analysis provides a measure for the degree of overlap between two (post-error vs. post-success, or left press vs. right press) neural response distributions, and it is independent of the firing rate of a neuron [55, 59]. For an isolated unit in one recording session, as an example, each trial in the session was first placed into either the post-error trials category or the post-success trials category. Then frequency histograms of the neurons' firing rates were obtained for post-error trials and post-success trials, respectively. Firing rate thresholds (ranging from the lowest to the highest selected

from among all recorded units) were used when creating the ROC curves. Each point (x, y) on the ROC curve corresponds to the two conditions, post-success and post-error. The x (or y) value represents the proportion of post-success (or post-error) trials that the firing rates were higher than the respective thresholds. Increased separation of firing rate distributions between post-success and post-error trails leads to an increased deflection of the ROC pushing toward the corner or away from the diagonal. The area under the ROC curve (AUC) provides a measure of the level of separation between the two compared distributions, the value of which ranges from 0.5 to 1. To interpret the separation level, a baseline ROC, and consequently AUC, is obtained from using randomly shuffled data. In this study, a bootstrap analysis was performed to estimate the chance-level AUC. For this purpose, neural data was randomly placed into one of the two categories for obtaining an AUC. The same was performed 1,000 times. The chance-level AUC was obtained as the average of the 1,000 sampled results. The farther an AUC value is from the chance-level AUC, or the closer an AUC value is to 1, the larger the distinction between the two (post-error vs. post-success, or left press vs. right press) neural response distributions.

The AUC_l and the AUC_r were used to measure differences in the distributions of neural responses between post-error and post-success trials among all left and right side responses, respectively. Specifically, when calculating AUC_l at a bin width of 100 ms, the units firing rates were calculated for all left side responses, and an AUC value was obtained. This procedure was repeated for each time bin to cover the 3 task periods. AUC_r was calculated similarly. By the same token, the AUC_s and the AUC_e were used to measure differences in distributions of neural responses between left and right directional choices among all post-success and post-error trials, respectively. The calculation for AUC_s and AUC_e was similar to the described above for AUC_l.

In this study, all analyses were performed using custom Matlab (Mathworks, Natick, MA) code.

Chapter 4

CORTICAL NEURAL RESPONSES TO PREVIOUS TRIAL OUTCOME DURING A DIRECTIONAL CHOICE LEARNING TASK

4.1 Introduction

Learning depends in large measure on adapting future actions based on previous outcomes. Several areas in the frontal lobe of primates appear to encode outcomes, including the prefrontal cortex (PFC), anterior cingulate cortex (ACC), ventral premotor cortex, and supplementary eye field (SEF) [29, 30, 31, 33, 86], as well as other medial frontal and motor areas [32, 72]. However, only recently have researchers started to address how trial outcomes may be encoded in single neurons in relation to future actions, especially during learning.

Neurophysiological evidence suggests that both the medial and lateral agranular frontal areas of rats, AGm and AGl, respectively, are involved in predicting trial outcome [37] and in learning [37, 53, 73, 121]. These findings are consistent with those showing that the rats lateral agranular cortex (AGl), which is homologous to the primary motor cortex in primates, shows considerable neuronal plasticity [44, 45, 48, 49, 51] and encodes information about task context [46, 47]. The medial agranular cortex (AGm) is probably homologous to one of the nonprimary motor areas in primates [38, 39, 74, 79]. Although some have argued for a homology of AGm to one of the primate prefrontal areas [34, 42], AGm's dense and direct projection to the spinal cord makes this idea unlikely. In addition to its neurons encoding predicted outcomes, lesions of AGm cause an increase in reaction time, which suggests an involvement in movement preparation [35]. Additionally, AGm neurons encode the action selected prior to movement onset in a value-based directional choice task [36].

Collectively, the published results point to AGm and AGl as candidates for encoding the outcome of previous trials, and suggest that this information plays a role in improving performance during learning. Accordingly, in order to study neural correlates of experience-based learning, I monitored the activity of single neurons in AGm and AGl of rats, as they learned a directional choice task. I studied the progression of neuronal activity from nave or pre-learning stages, through the learning stage and beyond. I found that single-unit activity was associated with two task factors: directional choice (left vs. right) and previous trial outcome (success vs. failure).

4.2 Materials and Methods

Male Long-Evans rats (n=12) were used in this Chapter. The animals weighed 50 grams upon arrival. They were handled daily and started training when they reached 300 grams to become familiar with the control paddles in the task apparatus prior to cortical array implant surgery. The 12 rats were trained extensively for an average of 72 sessions. Therefore, the rats were skilled and proficient with paddle pressing. Within the 12 rats, 6 rats (Rats C, D, E, F, G, and H) were used in behavioral and electrophysiological recordings; 4 rats (Rats I, J, K, and L) were used in video recording; 2 rats (Rats A and B) were used in both behavioral and electrophysiological recordings and video recording. Approximately three months later, at which time the animals usually reached 400 grams, they were implanted with microwire arrays. Upon recovery, the animals were placed in a Skinner box (Med Associate Inc.) and began learning the directional choice task while single unit neural signals as well as behavioral performance data were recorded simultaneously.

4.3 Results

Task performance and single-unit data from 8 rats (A, B, C, D, E, F, G, and H) were used for the analysis of neural modulation in relation to the two task-related factors: previous trial outcome and directional choice of the current trial. In this study, I considered the first paddle press within the response task period (Fig. 3.1C)when analyzing the directional choice factor.

The recording sessions with insufficient trials for statistical analysis were excluded. Units with firing rates below 1Hz were excluded from the analysis as well. For the units used in this study, average firing rats were 34.16±23.53 (spikes/s). A total of 41,840 trials from 232 neural and behavioral recording sessions were obtained from the 8 rats used in the analysis. Spikes were sorted offline after each recording session. Isolated units from each session were treated independently, which resulted in 1,058 unit records from 8 rats, including 514 from AGm and 544 from AGl (Fig. 3.1A). I recognize, however, that some cells remained the same from session to session, so the number of unit records does not correspond to the number of isolated neurons. The segregation of AGm from AGl cells was verified by intracortical microstimulation (see Materials and Methods). In addition, 6 rats (A, B, I, J, K, and L) were used in analyzing the movement characteristics such as start and end times and movement speed (see Materials and Methods).

4.3.1 Performance accuracy and response latency

The rat's performance accuracy, R, was obtained at the end of each recording session. Among the 8 rats used in this study (A, B, C, D, E, F, G, and H), 5 of them (A, D, E, G, and H) reached 80% or higher task performance accuracy. Specifically, 4 rats (A, D, E and H) reached 80% in about 21 sessions and Rat G reached 80% in

30 sessions. The other 3 rats (Rats B, C, F) reached performance accuracy of around 60% by the 20th recording session, and did not achieve 80% even in their respective last recording sessions. The learning curve for Rat A is displayed in Figure 4.1A as an example.

Three learning stages were identified according to the behavioral performance accuracy. The period after the rat's performance accuracy reached 80% or higher for at least 3 consecutive sessions was considered the learned stage. For the 3 rats (Rats B, C and F) who learned slowly, no experimental sessions could be placed into this category. Note also that some rats might have occasional fluctuations in performance accuracy around 80% in the learned stage. The learning stage was defined as during which the rats showed increasing trend in accuracy (t statistics, $p < 0.05$), e.g., from session 8 to session 21 for Rat A (Fig. 4.1A). The average accuracy increased by (25%) during the learning stage for the eight rats. The pre-learning stage was defined as the first several sessions in which the rats' performance accuracies fluctuated between 20% and 70% without displaying a clear and steady upward or downward trend (t statistics, $p > 0.05$). The lengths of each learning stage usually varied for different rats.

The response latency of each rat was computed for each session. The response latency was defined as the time between extension of the control paddles and the first paddle press by a rat. The response latency of rat A is shown as an example in Figure 4.1B and C. In summary, only occasional difference was found in response latency between successful and failed trials, and between post-success and post-error trials.

4.3.2 Kinematic analysis

Video sequences were captured for 6 rats (A, B, I, J, K, and L) while they performed the learning task. Rats A and B provided both neural and video data, while

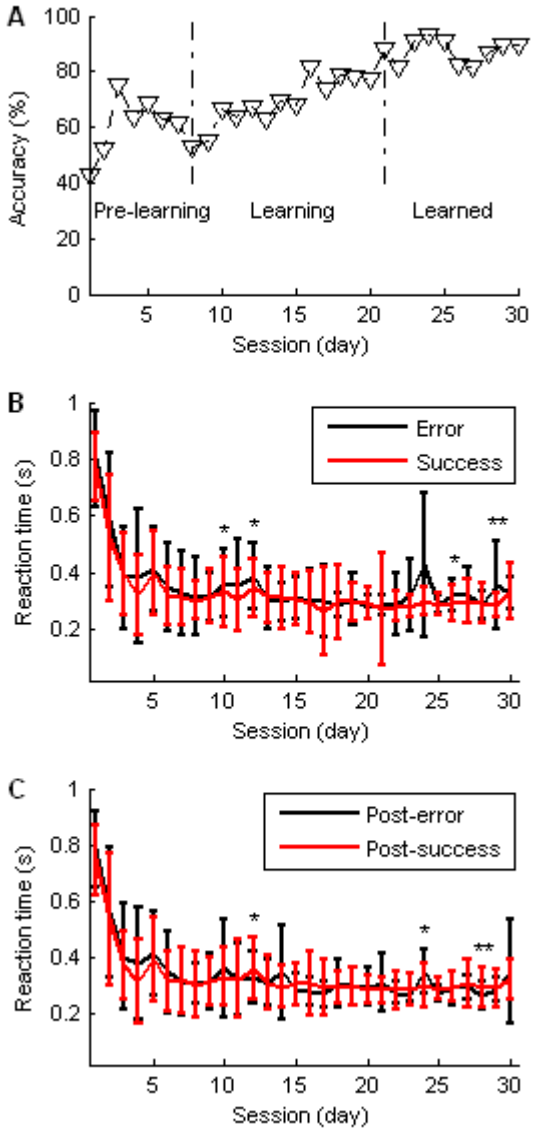

Figure 4.1: Examples of performance. A, Daily performance accuracy of rat A. Three learning stages were defined based on daily accuracy: pre-learning, learning, and beyond learning. B, C, Response latency for failed and successful trials (B) and post-error and post-success trials (C) of rat A in each recording session.

the other 4 rats (I, J, K, L) provided video data only. I analyzed the video sequences of the rats from the start of a trial (directional cue onset) to the time of the first control paddle press. For each of the 6 rats, the movement trajectories of the rat performing left and right press trials within a single session were first extracted. Figure 4.2A-C illustrates movement trajectories of rat J during one entire session where the x- and y-coordinates represent the positions of the rat's head over time from a front view. Using the definition of movement start and stop time defined earlier (Materials and Methods), from Figure 3B, C, we can see that the mean movement latency relative to cue onset was 249 ms ($\pm$ 20, SD) for left trials and 298 ms ($\pm$ 23) for right trials for rat J, respectively; the average end time was around 747 ($\pm$ 35) ms and 818 ($\pm$ 39) ms. respectively. The respective start/end positions of the rats could then be obtained based on the start and end time.

Figure 4.2D is an illustration of the movement start and end time as task learning progressed by session. Apparently, they decreased significantly during the initial 3 sessions (one-way ANOVA, $p < 0.05$) and reached a stable state on the 4th day, whereas movement duration decreased significantly (one-way ANOVA, $p < 0.05$) and reached a stable state by the 3rd day. The data suggest that only the initial trials during the first 3 or 4 sessions may have been modulated by movement kinematics. Similar analysis was performed for the remaining 5 rats (A, B, I, L, and K), and the same conclusion held true. The trend in those movement characteristics is in accordance with the trend of response latency profile in Figure 4.1B. Together, these data suggest that the rat's movement parameters became stable after only a few sessions. This finding probably reflects the fact that the rats were already trained for paddle presses in association with a cue light but without directional choice prior to their electrode implant. In addition to the sample results from some rats as shown in Figure 3A-D, movement start time across trials of all 6 rats was 342 $\pm$ 87 ms (mean

± 1SD), the end time was 829 ± 102 ms, and the movement duration was 487 ± 76 ms (Fig. 4.2E). Note that the start time and end time could vary from rat to rat. The data displayed in Figure 4.2D was typical for each of the 6 rats. Namely, the rats' movement parameters became stable after the first few sessions.

To further test if previous trial outcome may affect movement parameters, start and end time, movement duration, and movement start and stop positions were evaluated again as learning progressed. Video sequences of all trials from the 6 rats were used (A, B, I, J, K, and L). Movement start and end times and movement durations were compared between post-error and post-success trials using the U test. These parameters were found not affected by previous trial outcome ($p > 0.05$). Figure 4.3 is an example showing movement trajectories organized according to previous trial outcomes (error or success) in the x-coordinate. At each time point, the x-positions for post-error and post-success trials were compared using one-way ANOVA for the left press trials and right press trials, respectively. The comparison was repeated for each time point from cue onset to approximately 2.0 s after. No significant difference was found between post-error and post-success trials ($p > 0.05$). Similar observations held true for the y-coordinate. This result, together with the response latency measurements (Fig. 4.1C), supported the idea that the movement parameters in post-error and post-success trials did not differ significantly.

Thus, neither response latency nor movement kinematics varied according to the current or previous trial outcome. However, our data clearly show that the first 2-3 sessions (Figs. 2 and 3) included a confounding factor involving motor skill acquisition [37, 121], in addition to directional choice learning that is under study in this paper. Since our data revealed that the rat's movement parameters decreased mainly during the initial sessions, while the percent of correct trials remained low, I removed the

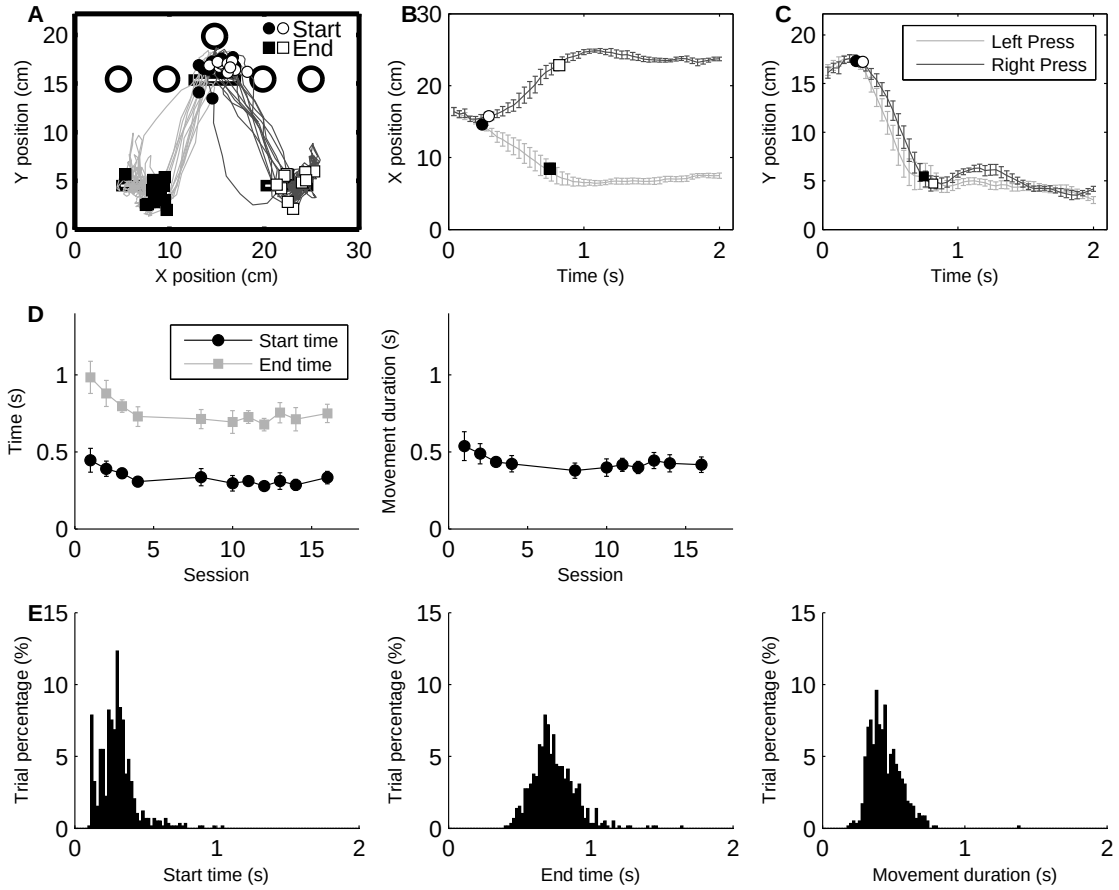

Figure 4.2: Movement characteristics. A, example movement trajectories from cue onset to paddle press of rat J. The background is the front view of the control panel facing the rat. The gray and the black curves represent the trajectories of left and right trials, respectively. The dots represent movement onset and the squares represent end of movement, which correspond to the rats head positions (see Materials and Methods). B, C, the x- and y-positions corresponding to movement trajectory in rat A along time. Error bars represent 1 SD. D, start time, end time, and movement duration as a function of learning sessions of rat I. Movement start and end time was longer in the first three sessions of learning and stays more stable afterwards. E, histograms of start time, end time, and movement duration for all 6 rats (A, B, H, I, J and K). Left, movement start time; center, movement end time; right, movement duration.

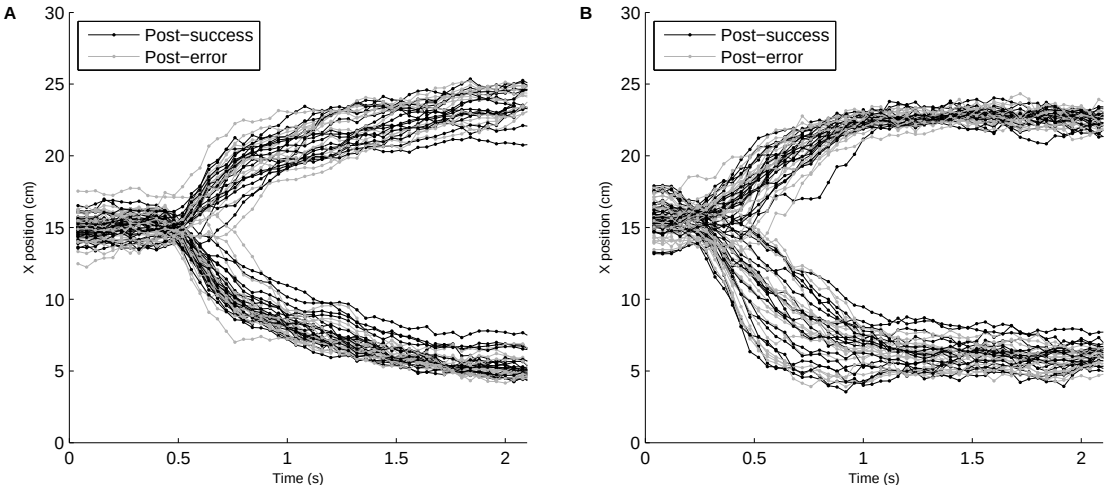

(a) (b)

Figure 4.3: Rat's movement was not dependent on the previous trial outcome. The x-coordinate is plotted as a function of time. Black lines and gray lines represent post-success and post-error trials, respectively. A, movement trajectories in an early session (session 5) of learning of rat L, i.e., in the pre-learning stage. B, movement trajectories in a later session (session 24) of rat K in the learning stage.

first 3 sessions of all rats from the data analysis performed next to eliminate the potential impact of motor skill learning.

4.3.3 Effect of previous trial outcome on performance accuracy

Behavioral task performance data were then evaluated as a function of previous trial outcome using all 8 rats A, B, C, D, E, F, G, and H. Trial outcomes immediately after a successful trial and a failed trial were considered by means of post-success accuracy, R_{ss}, and post-error accuracy, R_{es}, respectively. For each rat, the durations (in terms of sessions) of each of the three learning stages were normalized by the 8-rat averages. They are: 5.0 sessions for the pre-learning stage (excluding the first 3 sessions), 14.9 sessions for the learning stage, and 8.6 sessions for the beyond learning stage, respectively. The two measures developed in Materials and Methods, R_{ss} (post-

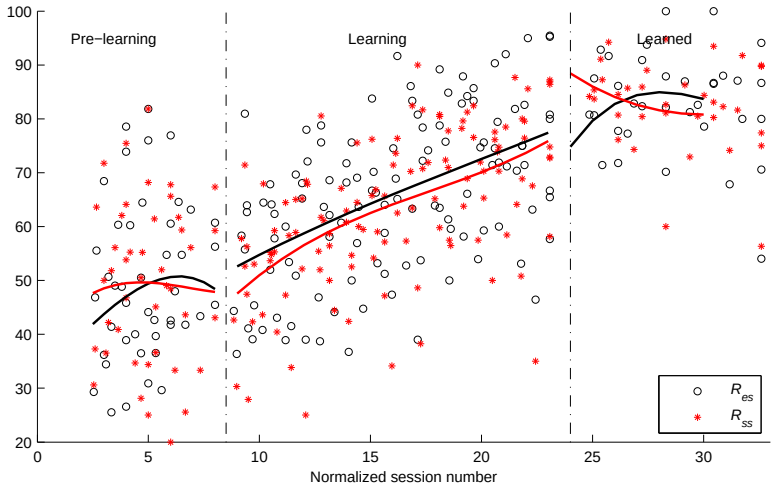

Figure 4.4: Behavioral performance in three learning stages for 8 rats. The x axis represents the normalized session number, and the y axis represents R_{es} and R_{ss} in black and red, respectively. The 4th order polynomial regression lines for R_{ss} and R_{es} are provided separately in each of the learning stages. In the pre-learning stage, R_{ss} and R_{es} first sharply increased and then leveled off. In the learning stage, R_{ss} and R_{es} continuously increased. In the learned stage, R_{ss} and R_{es} were almost flat. In learning stage, post-error accuracy R_{es} was greater than post-success accuracy R_{ss} (paired t test, $p < 0.05$).

success accuracy) and R_{es} (post-error accuracy), during each of the three normalized learning stages are summarized in Figure 5. Two respective 4th order polynomial regression lines are also shown for each learning stage to illustrate data trends. As shown in Figure 5, only during the learning stage that the post-error accuracy R_{es} (65.7% $\pm$ 14.9%) was slightly higher than the post-success accuracy R_{ss} (63.5% $\pm$ 14.2%) with statistical significance (paired t test, $p < 0.05$).

4.3.4 Neural activity modulated by task factors

For this analysis, I used neural data from 8 rats (A, B, C, D, E, F, G, and H). Among the entire set of 1,058 isolated unit records of the 8 recorded rats, excluding the initial three recording sessions, a total of 918 isolated unit records were included

in the following neural analysis (AGm: n = 464, AGl: n = 454). Among the 918 unit records, 88.3% (n = 811) were found to be task-related, including 86.2% (400 out of 464) of AGm and 90.5% (411 out of 454) of AGl units, respectively. Neural activities of these unit records were first inspected using the perievent time histograms (PETHs). To analyze rats neural correlates during the directional choice learning, two task-related factors were investigated: (1) directional choice (left press or right press) of the current trial, and (2) previous trial outcome (success or failure).

Two examples of neural modulation represented in PETHs are shown in Figures 4.5 and 4.6 for an AGl neuron and an AGm neuron, respectively. Note that for clarity, 1/6 of the total trials in a session are uniformly sampled and displayed here.

Figures 4.5 and 4.6 show example records in which the average firing rate was modulated by both the directional choice and previous trial outcome in the cue-on and response periods. They also show that neural modulations were stronger in some task periods than in others (top panels in Fig. 4.5 and 4.6). This property suggests that the firing rates of these single units encode two factors, directional choice and previous trial outcome, and do so dynamically.

To gain insight into these two factors, I evaluated them separately using ROC analysis. The AUC's over time were calculated using a time bin of 100 ms that was slid in 20-ms steps. The time coverage spans from 1.0 s prior to cue onset to 3.0 s after cue onset, which corresponds to the entirety of the 3 task periods (see Fig. 3.1C). The AUC_l and the AUC_r provided measures of differences in the distributions of neural responses between post-error and post-success trials among all left and right side responses, respectively. The AUC_s and the AUC_e provided measures of differences in distributions of neural responses between left and right directional choices among all post-success and post-error trials, respectively. Results of the AUCs over time are illustrated in the center panels of Figures 4.5 and 4.6.

The first set of AUCs, AUC_l and AUC_r, showed that both left trials and right trials were affected by previous trial outcome. And for the two example units (center panels of Fig. 4.5 and 4.6), the firing rates of post-error trials was lower than those of post-success trials. The second set of AUC's, AUC_e and AUC_s, showed that post-error or post-success trials still carried directional choice information.

4.3.5 Population analysis

Two-way ANOVAs were performed to study how single unit firing rates changed dynamically over all three task periods (pre-cue, cue-on, and response) as a function of the two task factors: previous trial outcome and the directional choice of the current trial. I examined the statistical significance of the two task factors by the following three p-values. Two single p-values were considered for the main effects: p_1 for directional choice, p_2 for previous trial outcome, and the additional p-value p_3 for two-factor interactions between directional choice and previous trial outcome.

The two-factor interaction terms were obtained for each unit record at each of the 18 time points by two-way ANOVA. To inspect the interacting effect of the two task factors, the number of unit records corresponding to a statistically significant interaction ($p_3 < 0.01$) was accounted for at each of the 18 time points. It turned out that during the three task periods, few AGm and AGl unit records exhibited significant two-factor interactions. On average (for time points 1-18), 2.7% (n = 10.9) and 2.0% (n = 8.1) of the task-related AGm and AGl unit records, respectively, were modulated by the interaction between directional choice and previous trial outcome. These results indicate that the interacting effect of the task factors on the neural firing rates was insignificant for most task-related units during the pre-cue, cue-on and response task periods.

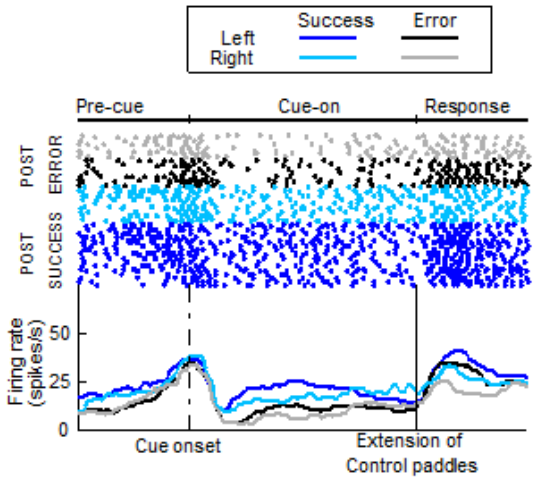

(a)

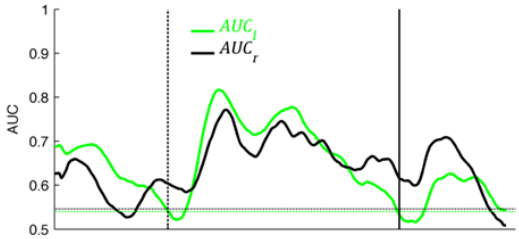

(b)

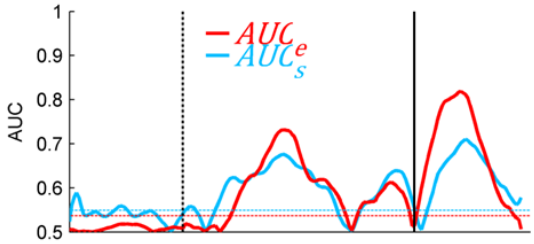

(c)

Figure 4.5: Example AGl unit and its spike raster of rat D isolated from channel 7 on the 12th recording session. The x axis is the time course with event markers. The top panel: spike raster plots from individually recorded trials and the average firing rates. The center panel: AUCs to compare differences in neural responses between post-success and post-error trials for a left (green) or right (black) directional choice, respectively. The bottom panel: AUCs to compare differences in neural responses between left and right directional choices after a successful trial (blue) or an error trial (red), respectively. The respectively chance level AUC values are shown in dashed lines in the center and bottom panels.

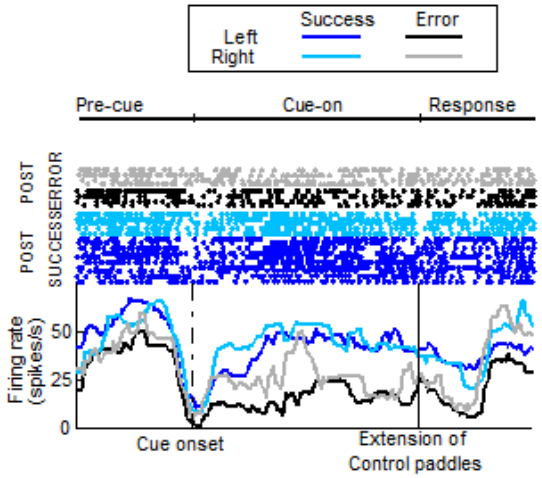

(a)

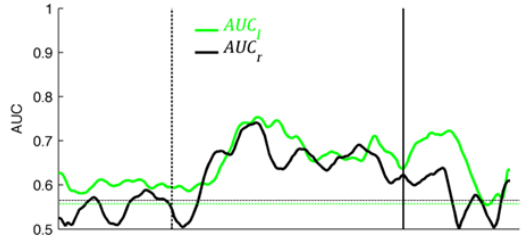

(b)

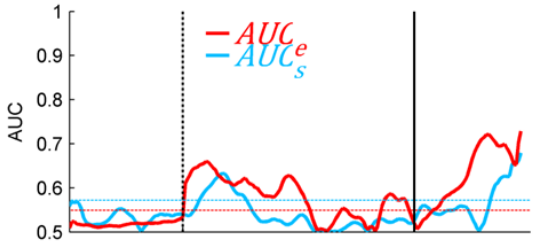

(c)

Figure 4.6: Example AGm neuron spike raster for Rat E isolated from channel 14 on the 16th recording session. The convention is the same as in Figure 4.5.

Next, I show that neural modulations encoding the two task factors varied over time. From Figure 4.7A, a large number of AGm unit records was modulated by previous trial outcome in the pre-cue (34.8%, n = 139.0), cue-on (38.8%, n = 155.0), and response (25.9%, n = 103.7) task periods. The largest number of unit records encoding previous trial outcome was found at the 8th time point indicated by letter "c" (400 − 900 ms after cue onset, 51.2% of units, n = 205). Also, an increasing number of unit records was significantly modulated by directional choice after cue onset and peaked at 55.0% (n = 220) in the 17th time point during the response task period. Similarly for AGl units, previous trial outcome was modulated by previous trial outcome in the pre-cue (39.1%, n = 160.5), cue-on (42.2%, n = 173.3), and response (29.2%, n = 120.2) task periods (Fig. 8B). The largest number of unit records encoding previous trial outcome was found at the 8th time point indicated by letter "d" (52.5% of units, n = 216). Also, an increasing number of unit records was significantly modulated by directional choice after cue onset and peaked at 57.2% (n = 235) in the 17th time point during the response task period. Therefore, the neural activity in the cue-on task period, especially the beginning portion, appeared to be modulated by previous trial outcome. As shown by the dark lines in Figures 8A and B, a large portion of both AGl and AGm unit records was encoding the previous trial outcome within the cue-on data window. Examining the cue-on data period more closely, it is interesting to note that starting from the 11th (for AGm) or the 13th (for AGl) time point and onward, a larger number of AGm or AGl unit records responded to directional choice than to the previous trial outcome.

I further investigated the distributions of p-value pairs of all task-related AGm and AGl unit records based on the two task factors at the 8th time point corresponding to points "c" and "d" in Figures 4.7A and 4.7B, respectively. The corresponding results are shown in Figures 8C and D. The same calculation was then conducted for each

of the time points from 5 to 18 as for point 8. Only a small portion of the task-related AGm and AGl unit records were modulated by both directional choice and previous trial outcome as main effects during the cue-on and response task periods (10.7%, n=42.8 for AGm and 9.7%, n=40.1 for AGl), respectively. This indicates that a single unit was predominately modulated by a single factor at a time.

4.3.6 Previous-outcome coding in the cue-on period

Since both AGm and AGl neural modulation was most affected by previous trial outcome during the initial part of the cue-on window (dark lines in Fig. 4.7A, B), which also corresponds to the period when the rats movement was stereotypical with little variation (Fig. 4.2), I focused our analysis on this time period. To do so, I used the previous trial modulation measure,I_1, which is a 1×100 vector covering the cue-on task period and providing a measure of discrimination in neural firing rates between post-success and post-error trials. Since this is a collective account of all task-related units and because the properties of AGm and AGl resembled each other closely, I pooled AGm and AGl units for this analysis.

The differences in firing rates between post-success and post-error trials were strongly affected by previous trial outcome at the time of the cue-on data window (Fig. 4.8A). The time bin τ_1 at which I_1 achieved the highest value was computed for each unit. From Figure 4.8B, the largest number of units (14.4% of total task related numbers, n = 117) was found at τ_1=600 ms after the cue onset. And 64.0% of (n = 519) units had τ_1 within the cue-on data window (Fig. 4.8B). This finding provides further support for the idea that the greatest degree of modulation encoding the previous trial outcome occurred during the cue-on data window.

For the 811 task-related AGm and AGl unit records, the average $I_1^i (i = 11, \cdots, 45$, corresponding to the cue-on data window) value over the cue-on data window was

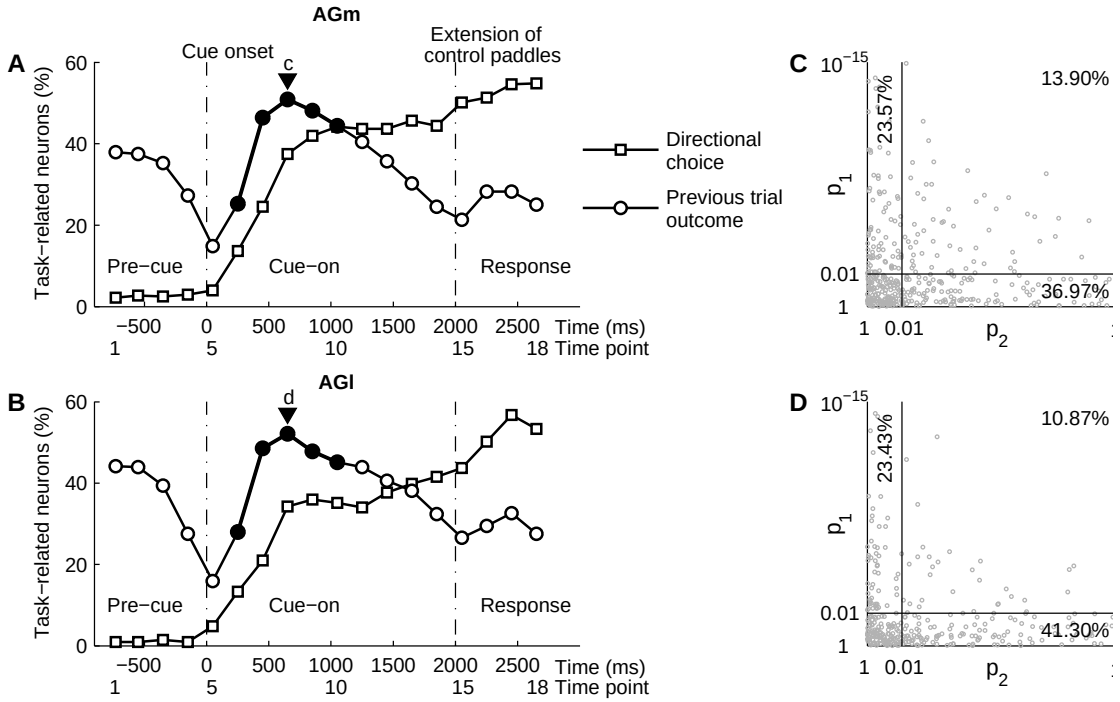

Figure 4.7: Summary of task-related neurons (n = 811) and their dynamic modulations according to the two task factors: directional choice (left press or right press) or previous trial outcome (success or error). A, B, Dynamic representations of the percentages of task-related neurons that showed significant modulation to the two task factors: directional choice (squares) and previous trial outcome (circles) using two-way ANOVA (see text in Results), respectively. The solid circles represent the fractions of neurons modulated by previous trial outcome during the cue-on data window. C, D, Scatters of p value pairs of each task-related neuron. C, point "c" in panel A corresponds with the 8th data point during the cue-on task period. 37.0% (n = 149) of the AGm neurons were encoding previous trial outcome, 23.6% (n = 95) were encoding directional choice, and 13.9% (n = 56) were encoding both. D, point "d" in panel B corresponds with the 8th data point during the cue-on task period. 41.3% (n = 171) of the AGl neurons were encoding previous trial outcome, 23.4% (n = 97) were encoding directional choice, and 10.9% (n = 45) were encoding both.

denoted as $\bar{I}_1$. The histogram of the $\bar{I}_1$ values for all task-related units is displayed in Figure 4.8C. Recall that $I_1 = \frac{f_E(1)-f_S(1)}{\max(f_E(1),f_S(1))}$. The finding that the $\bar{I}_1$ was less than 0 for the largest fraction of these units (73.8%, n = 599), indicates that most units had greater activity in post-success trials than in post-error trials, thus encoding positive outcomes. Figure 4.8A, B shows that differences in neural firing rates between post-error and post-success trials changed dynamically during the time course of a trial, with the differences being most pronounced during the cue-on data window. Furthermore, the firing rates of most task-related units decreased after the rat made an error.

4.3.7 Previous-outcome coding and performance accuracy

Next, I examined how performance accuracy correlated with the observed neural activities. Given that previous outcomes and chosen response direction did not commonly have interactive effects, it was adequate to analyze the factors of previous outcome and chosen direction independently. The firing rates of AGm and AGl units in the cue-on data window (from 200ms to 900ms after cue onset, Fig. 3.1C) were thus inspected using one-way ANOVA. The units showing significant neural modulation ($p < 0.01$) in the cue-on data window in response to previous trial outcome were classified as previous outcome selective, and unit records with this property were analyzed separately for AGm and AGl. A total of 417 unit records including 52.2% (209 out of 400) of AGm unit records and 50.6% (208 out of 411) of AGl unit records encoded the previous outcome.

Of the eight rats included in this study, their behavioral task performance accuracy over recorded sessions ranged from 33.4% to 92.1%. This distribution was equally divided into 12 intervals ranging from 35% to 90% in 5% increments. The units recorded in each session were placed into one of these 12 intervals. The intervals

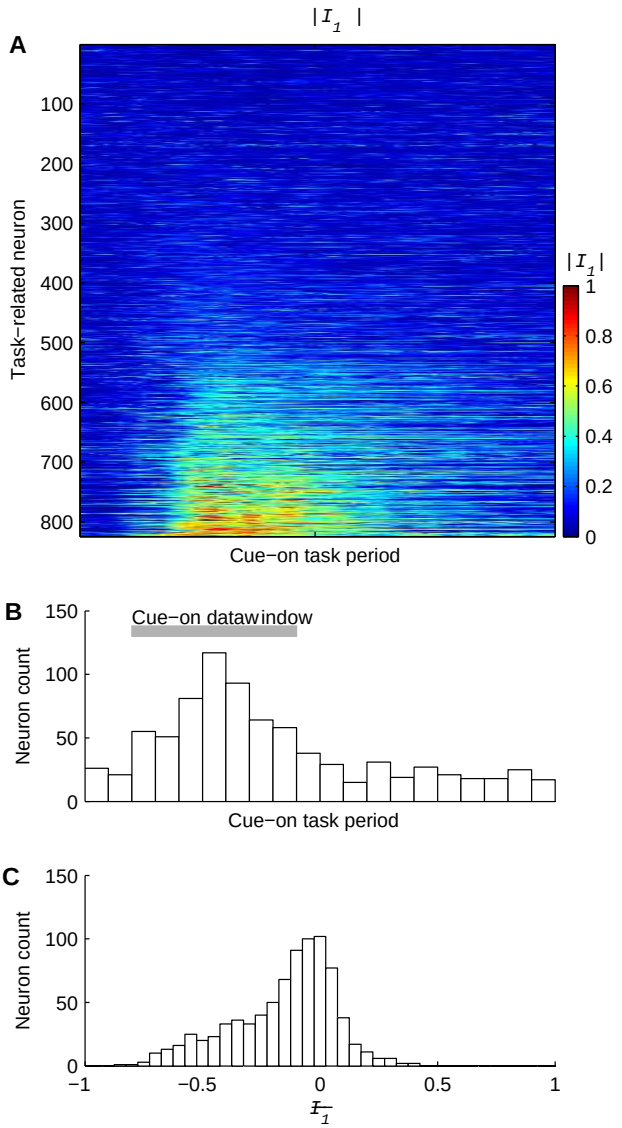

Figure 4.8: Summary of previous trial modulation measure I_1 vector over the cue-on task period for all task-related neurons (n = 817). A, The component-wise absolute values of the I_1 of each task-related neuron during the cue-on task period. Neurons were sorted in ascending order according to the absolute values of $\bar{I}_1$. B, Distribution of τ_1 at 100 ms time bins. C, The histogram of all task-related neurons according to $\bar{I}_1$.

with fewer than 15 units were excluded from this analysis, resulting in performance accuracies ranging from 40% to 85% for final examination. As a result, 37.6 ± 18.2 (mean ± SD) unit records in each of the 10 intervals for AGm and 37.9 ± 18.0 unit records for AGl. The results from AGm and AGl are plotted separately in Figure 4.9. In the cue-on data window, the fraction of previous trial outcome selective units were found strongly correlated with performance accuracy for both AGm and AGl units (correlation coefficient, r = 0.91 for AGm, and r = 0.96 for AGl, both of which were highly significant, $p << 0.001$).

To answer the question of whether there is any significant difference between AGm and AGl units in percentages as they were modulated by performance accuracy shown in Figure 4.9, I performed a paired t test. No significant difference was found in the percentages of AGm and AGl unit records (p=0.70).

4.3.8 Previous-outcome coding across the three learning stages

To examine previous-outcome coding across the three learning stages, I computed the AUC's between post-error trials and post-success trials. For each previous outcome selective unit, firing rate from each trial in the cue-on data window (200-900 ms after cue onset) was obtained and placed into either the post-error or the post-success category, respectively. All trials within a session were used to obtain the AUC's, which is based on the neural response distributions of post-error or post-success trials. This process was repeated for all previous outcome selective units.

During the pre-learning stage, 193 unit records were obtained (AGm: n = 88, AGl: n =105) of which 42.5% were previous outcome selective (AGm: n = 42, 47.7%; AGl: n = 40, 38.1%). During the learning stage, 487 unit records were obtained (AGm: n = 244, AGl: n =243), and 55.0% of them were previous outcome selective (AGm: n = 133, 54.5%, AGl: n = 135, 55.5%). During the beyond learning stage,

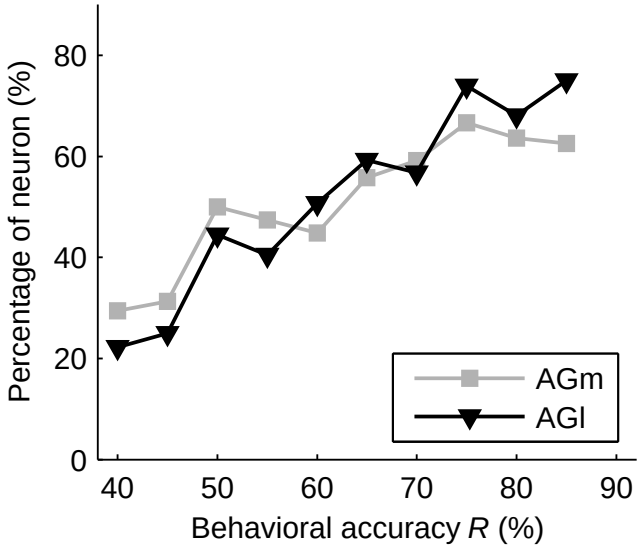

Figure 4.9: The percentage of previous trial outcome selective AGm and AGl neurons as a function of daily accuracy R. Break-downs of 10 behavioral performance intervals from 40% to 85% were used. The percentage of previous trial outcome selective neurons in each interval was calculated as dividing the number of previous trial outcome selective neurons by the total number of task-related neurons in the interval. No significant difference was found between AGl and AGm neurons for the 10-point data series (paired t test, p = 0.6969).

137 unit records were obtained (AGm: n =71, AGl: n =66), of which 48.9% were previous trial outcome selective (AGm: n = 34, 47.9%, AGl: n = 33, 50.0%).

The chance-level AUC value was 0.55. The largest deviations of AUC values from 0.55 (t test, $p < 0.01$; Fig. 4.10) were associated with the learning stage (0.81±0.10 for AGm, 0.83±0.09 for AGl), which was statistically significant by pair-wise comparisons between the learning stage and the other two stages (one-way ANOVA, $p < 0.05$). The AUC values were also significantly larger than the chance-level AUC for units

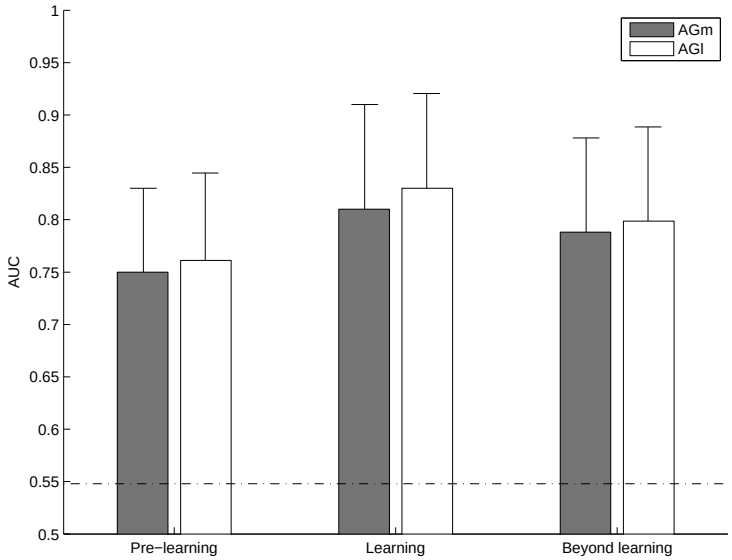

Figure 4.10: The means and standard deviations of AUC values to measure differences in neural responses between post-error trials and post-success trials in the pre-learning, learning, and beyond learning stage. The most significant distinction was found to be during the learning stage for both AGm and AGl units, as compared to the pre-learning and beyond learning stages. Dashed lines represent the neutral state (chance-level AUC value). The farther the AUC values diverge from the chance-level, the larger the differences in the firing activity between post-error and post-success trials.

recorded in the pre-learning (0.75±0.08 for AGm, 0.76±0.08 for AGl; t test, $p < 0.01$) and beyond learning (0.79±0.09 for AGm, 0.79±0.09 for AGl; t test, $p < 0.01$) stages. Thus the most significant improvement in performance accuracy (Fig. 4.4) and the most significant neural modulation by previous outcome (Fig. 4.10) occur during the learning stage. This suggests a positive correlation between the firing rate modulation by previous trial outcome and the behavioral performance adaptation during the learning stage.

4.4 Discussion

A rat model was used in this report to examine behavioral and neural responses during learning of a directional choice task. Two task related factors (previous trial

outcome of either success or failure; current trial directional choice of ether left or right) were analyzed in association with the rat's neural activity and behavioral learning performances. Our study revealed that the recorded AGm and AGl units encoded both current trial directional choice and previous trial outcome during the time course of a single trial (Fig. 4.5-4.7). Our major findings were: (1) in the time course of a trial, a large fraction of recorded individual AGm and AGl units were modulated by previous trial outcome especially in the cue-on data window (Fig. 4.5-4.8); (2) more units had greater activity post successful trials than post error trials in the cue-on data window (Fig. 4.8C); (3) the number of previous trial outcome selective units was highly correlated with the rat's behavioral performance accuracy (Fig. 4.9); and (4) for those previous trial selective units, the differences in the neural responses between post-error and post-success trials were the greatest during the learning stage when compared to trials before and after learning (Fig. 4.10). These results suggest that the AGm and AGl of the rat frontal cortex are not static but adaptive at fine time scales of seconds or sub-seconds. Our data may further suggest that modulations in those units contributed to retrospective information processing for rats during the learning process.

4.4.1 Task factors and single units

In our experiment, other factors that might also affect recorded neural activity are summarized as follows. All the rats used in the study learned the contingency between a light cue and a paddle press during pre-training prior to learning the directional choice task. Furthermore, the variations in the rat's kinematics measured by response latency (Fig. 4.1B, C) and movement characteristics (Fig. 4.2) quickly reduced to an insignificant level during the pre-learning stage. Hence the data used in this analysis excluded the first 3 recording sessions (refer to discussions on Fig.

4.2) but only included the sessions when rat's kinematics became stable. Given the above considerations of those unlikely confounding factors to elicit additional neural responses in the areas I recorded from, previous trial outcome and directional choice are considered the two primary task factors.

Additionally for the issue of chronic recording from single units, one analysis of macaque monkeys suggested that about one third of the chronically recorded primary and premotor cortical neurons retained their isolation across sessions [60]. [61] suggested that 50% of the original units were stable through 1 week and 10% were stable through 2 weeks based on their motor cortical chronic recordings from two monkeys. In this study, I treated each isolated unit from each recording session as an independent sample, and our analysis did not rely on keeping track of the identity of each neuron from session to session for two reasons. First, all our major results (Figures 4.6-4.9) were based on single unit firing rates computed over one recording session when isolated units were believed to be stable during the hour long experimentation. Second, the results were actually collective accounts of a neural population, similar to that used previously [91, 121]. The results were not about neural adaptation of a single unit before and after learning, but rather they were to describe how a population of multiple single units adapted as behavioral learning progressed.

4.4.2 Distributed neural modulation of previous outcome

Significant evidence from primate and rodent studies indicated a widespread neural modulation in response to previous outcome during learning. Trial outcome as a transient event was shown clearly encoded in single unit activity in PFC [91, 92], ACC [70, 71], striatum [92], and hippocampus [67]. The signal was sustained in the inter-trial interval and carried over to the next trial, which may have contributed to linking past outcomes with future actions [68]. Additional evidence was also avail-

able in human studies [69]. Among those brain areas, the PFC has been regarded as an important node playing the role of top-down control of error processing, it may require well-coordinated participation from a large network of cortical and even subcortical areas. For instance, the monkey's premotor cortex was shown to be involved in abstract rule learning [55], and the ventral premotor was proposed for processing and evaluating the behavior of previous decisions [99]. Our results for the first time pointed to the rat's AGm and AGl for their involvement in processing previous outcome in relation to outcome-dependent behavioral adaptation.

By reviewing evidence based on cytoarchitectonics, topology, and corticostriatal projection of rats with primates, [75] did not consider rat having a "granular" prefrontal cortex. While others disagree with this theory [34, 80, 81], some researchers referred to the anterior cingulate, prelimbic, and infralimbic areas of rats as the prefrontal cortex and reported sustained trial outcome related signals in those areas, or simply the rat's PFC [91]. Even though the part of the AGm that we recorded from does not overlap with the PFC in the sense just described, there has been clear evidence that the AGm has reciprocal connections with the dorsomedial prefrontal cortex (dmPFC) [41]. Specifically, it takes afferent projections from two subregions of the dmPFC: the dorsal prelimbic cortex and pregenual anterior cingulate cortex [82, 98]. And AGm is one of the few non-limbic cortical regions that project back [78]. Additionally, the rat's AGm has been proposed to be possibly homologous to the premotor cortex, supplementary motor area and frontal eye field in primates [41, 43, 79], and to be a multimodal association area [41, 43]. But agreement has not been reached for a clear homology between the rat's AGm and the primate's counter parts. Since the rat's AGm projects to the spinal cord, it is adequately identified to be homologous to one of the nonprimary motor areas in primates [39, 74] while the specific identification of which one remains conjectural. On the other hand, the

rat's AGl has been considered homologous to the primary motor cortex [39, 77], and is connected reciprocally with AGm [41, 43, 76]. It is therefore not surprising that previous trial outcome information could be conveyed to AGm and AGl to mediate the rat's future choice behavior.

4.4.3 Neural correlates to behavioral error correction

We recorded rat's neural activity in the AGm and AGl areas along with rat's behavioral performance simultaneously during the entire process of rat's learning the directional choice task: from pre-learning stage, through the learning stage and beyond. This has given us the unique opportunity to correlate neural adaptation in rat's AGm and AGl areas with their behavioral performance accuracy. Specifically I found that the number of previous trial selective neurons was positively correlated with the rat's learning performance and that during the learning stage, the difference in neural responses between post-success and post-error trials was the greatest, compared to trials before and after learning.

[91] recorded rats' dorsomedial PFC and primary motor cortical neurons during a reaction time task. [92] recorded PFC neurons in monkeys learning an arbitrary stimulus-response association task. Both studies found that the firing rates of a fraction of the recorded single neurons were modulated by previous trial outcome. Furthermore, their study found about half of the recorded PFC neurons increased their firing rates in post-success trials than post-error trials. For most of the recorded primary motor cortical neurons in [91], the respective firing rates increased in post-success trials than the post-error trials.

Even though our experiment is different from the reaction time or arbitrary stimulus-response association tasks in [91] and [92], respectively, I also observed strong neural modulation by previous outcome in a large number of AGm and AGl neurons.

However, I have also realized differences of our results from theirs. Specifically, I found about 70% AGm and AGL neurons had higher firing rates in post-success trials than in post-error trials, while 30% had higher rates in post-error trials than in post-success trials. These specific differences in the number of modulated neurons and the specific modulation trend may be due to variations in experimental conditions and specific recording sites. Nonetheless, these results together suggest that several areas in the frontal cortex such as the AGm, AGl, and the PFC are important in processing and passing error related information. As [68] pointed out that the widespread presence of signals in different brain areas encoding previous outcome may not imply that they serve the same functions. A better understanding of how information is processed at each node requires further investigation about how exactly these areas coordinate to process information from past experience in order to guide future actions.

Finally, our results together with previous studies demonstrate that neural adaptation to previous trial outcome may be a part of a general mechanism for learning and such neural adaptation may involve a distributed system of several well-coordinated brain areas.

Chapter 5

CORTICAL NEURAL MODULATION BY PREVIOUS TRIAL OUTCOME IS A CONTRIBUTING FACTOR IN TRIAL-AND-ERROR LEARNING SPEED

5.1 Introduction

Learning to acquire new information or knowledge is essential for survival. We usually learn from both positive and negative outcomes after taking certain selective actions such that positive outcomes are reinforced while negative outcomes are avoided by adjusting action selection. The means used by individuals to learn from previous errors varies as a result of many factors including adopted strategy and individual experience. Recent studies reported that subjects usually learn a task in varied length of time [110, 111, 112, 113]. Human studies have provided ample evidence that individual difference in cognition-related behavior is correlated with prefrontal structures and their functions [114, 115, 116, 117, 118]. Yet, existing results were mostly obtained through the means of fMRI, TMS, and EEG. How relationships between single unit neural activity and behavior vary for individuals, however, has not yet been systematically investigated.

I used a rodent model to understand cortical neural correlates to learning and especially what at single unit level sets apart fast learning from slow learning. The medial agranular cortex (AGm) and lateral agranular cortex (AGl), homologous to one of the non-primary motor and the primary motor cortex of primates, respectively [38, 39, 41, 79], may encode information other than movement kinematics [46, 47], and involve in high level cognition [48, 49, 50, 51]. As a part of the frontal cortex, the rodents AGm and AGl areas are being studied and their functions are gradually becoming clear [34, 35, 36]. As shown in Chapter 4, neurons in rats' AGl and AGm encode previous trial outcome.

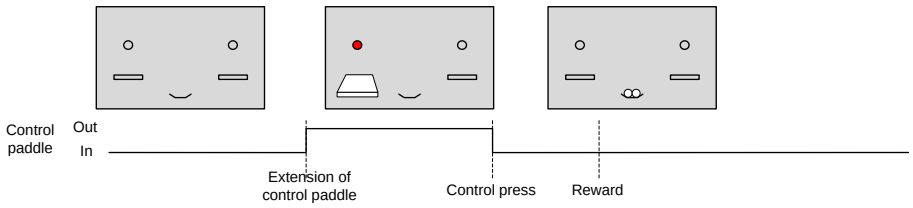

Figure 5.1: Training task.

To investigate the behavioral and neural activity in relation to a learning process in different individuals, I adopted the following experimental approach: (i) record single-unit activity in AGm and AGl areas of rats, when they performed a directional learning control task by trial-and-error; (ii) analyze behavioral performance and separate the animals into fast and slow groups; and (iii) analyze neural activity modulated by directional choice and previous trial outcome. Our analysis shows that the neural activity in fast and slow rats differed significantly in representing task factors.

5.2 Materials and methods

5.2.1 General

The subjects, experimental procedure, surgery, and data acquisition follow the same convention as described in Chapter 3. Briefly, 10 male Long-Evans rats arrived at two weeks after birth, weighing 50 grams. They were handled daily and started training when they reached 300 grams. Figure 5.1 shows an example training trial. There are two lights and two paddles. One of the two paddles will extend at the same time when the corresponding cue light is on. The rat is given a long time to press the paddle to receive a reward pellet (mixture of grain pellets and sugar pellets). Ten rats were trained for an average of 72 sessions and usually achieved 90% of training accuracy in 15 sessions.

Approximately after the rats weighed more than 400 grams they were implanted with microwire arrays. The rats started the directional choice task upon recovery from surgery.

5.2.2 Learning period

To define a proper learning period for each rat, linear regression was performed on performance accuracy in any consecutive five sessions and regression slope was obtained. The slope reflected whether the rats showed an improving trend (slope larger than zero) or not (slope smaller or equal to zero). To efficiently evaluate the learning period, starting and ending points were characterized. The starting point of the learning period was defined as the first session from which the slope was non-negative for at least two consecutive sessions. The end point of learning was defined as the session that the rat reached 80% for three consecutive sessions, or the last session if the rat did not reach 80% steadily. The sessions between the starting and ending points are considered a learning period. Neural analysis was performed from the sessions in the learning period.

5.2.3 Definition of fast and slow rats

Two criteria were used to place the rats into one of the two categories of either fast or slow learning: (1) the number of sessions that the rats took to reach an accuracy of 70% steadily. This measure reflected the rats ability to achieve a high accuracy. (2) the averaged 5-session learning slopes during the entire learning period. This measures the learning ability during the learning period.

5.2.4 Neural firing rate vs. two task factors

The major procedures of recording, data analysis were the same as described in Chapter 3. In this chapter, the effect of the two task factors (directional choice and previous trial outcome) were analyzed using two-way ANOVAs. Each task-related neuron was taken into account. A window of 500 ms traversed the timeline in 200 ms steps starting from the pre-cue task period to the end of the response task period. For each trial, the firing pattern in a trial timeline (including three task periods) was represented by an 18-point data series, as described in Chapter 4. Two-way ANOVA could then be applied at each time point. The significance was assessed by the p values obtained with the significance level chosen as $p < 0.01$.

5.3 Results

5.3.1 General

Task performance data and single-unit data from 10 rats (A, B, C, D, E, F, G, H, M and N) were used for the analysis of neural modulation in relation to the two task-related factors: previous trial outcome and directional choice of the current trial. As the results shown in Chapter 4, a handful of sessions at the beginning might involve in motor skill learning. As a result, in the following analysis, both the behavioral and neural data in the first three sessions were removed.

5.3.2 Fast and slow rats, learning period

Behavioral performance was analyzed first for each of the ten rats. The rats usually showed distinct learning characteristics. Some rats increased performance accuracy right after a few sessions since they started the directional choice task while some rats took a longer period to learn. Starting and end points of learning period

were calculated for each rat. On average, the starting point was at 6.3 sessions, and the ending point was at 24.8 sessions.

According to the two criteria, 5 of the 10 rats (A, D, E, H, and N) were identified as fast rats and the other five (B, C, F, G, and M) slow rats (Fig. 5.2). According to the data, the fast rats achieved accuracy greater than 60% in the 15th session, and the slow rats accuracy was lower than 60% in the 15th session. The fast and slow rats improved behavioral performance during the learning process with an average starting point at 5.6 sessions. The slow rats showed a longer period prior to learning (average starting point at 7.0 session). The difference between the performance accuracy of the two groups was tested using one-way ANOVA. From the 7th session, the fast rats' accuracy was significantly higher than the slow rats ($p < 0.05$).

However, by looking at the average accuracy, the slow rats did not seem improving immediately since the 7th session. The average learning rate in the learning period was calculated using 1st order linear regression. The accuracy of slow rats in the first 12 sessions (named SP rats) remained leveled with the learning rate being 0.38 (percent/session). The fast rats exhibited steady improvement since the starting point (FL rats). Similarly, the slow rats improved steadily after 12th session. The learning rate is 1.73 and 1.96 (percent/session) for the FL and SL rats, respectively. This shows that the fast rats started to improve once into the learning period. However, the slow rats experienced an extended period prior to learning.

Here, the age of rats and training experience were not affecting the learning results. The fast and slow rats started around similar age (fast rats started on 132.2 ± 39.6 and slow rats started on 154.4 ± 42.3, no statistical significance, one-way ANOVA, p = 0.42). The rats were extensively trained with paddle pressing prior to learning the directional choice task and reached accuracy higher than 90%. The fast rats were trained for 71.6 ± 41.6 sessions and slow rats were trained for 72.6 ± 34.8 sessions

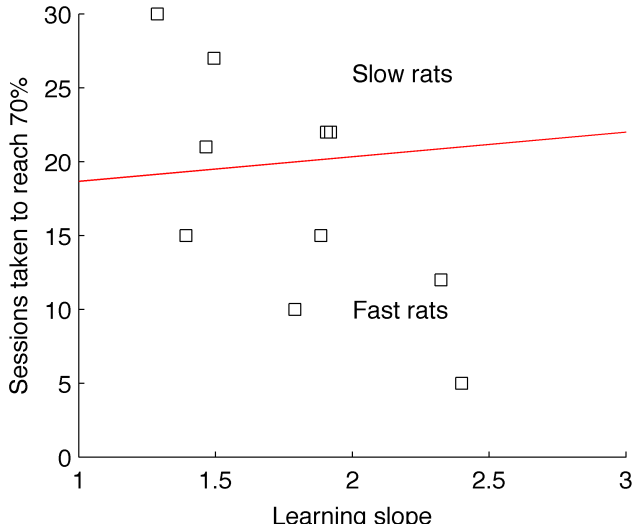

Figure 5.2: Averaged learning slope and number of sessions taken to reach 70% of fast and slow rats. X axle, averaged 5-session slope during the learning period; Y axle, number of sessions taken to reach 70% steadily.Red line indicates the separation of fast and slow rats.

(no statistical significance between two groups, p = 0.68, one-way ANOVA). Note that, although the fast rats and slow rats seemed to differ in the learning rate at the beginning of learning the directional choice task, they did not differ during conditional training (left panel of Fig. 5.3).

5.3.3 Neural modulation by directional choice and previous trial outcome

To compare the neural activity in fast and slow rats effectively, neurons recorded in the learning period of each rat were used in neural analysis. A total of 684 single unit neural records were obtained from slow (381) and fast (303) rats in the ten rats. 591 of them were task-related (325 from slow rats, 266 from fast rats). As demonstrated in Figure 4.7 and Figure 4.9 in Chapter 4, no significant difference existed between AGm and AGl neurons. Therefore, I pooled AGm and AGl neurons together in the neural analysis performed in this chapter.

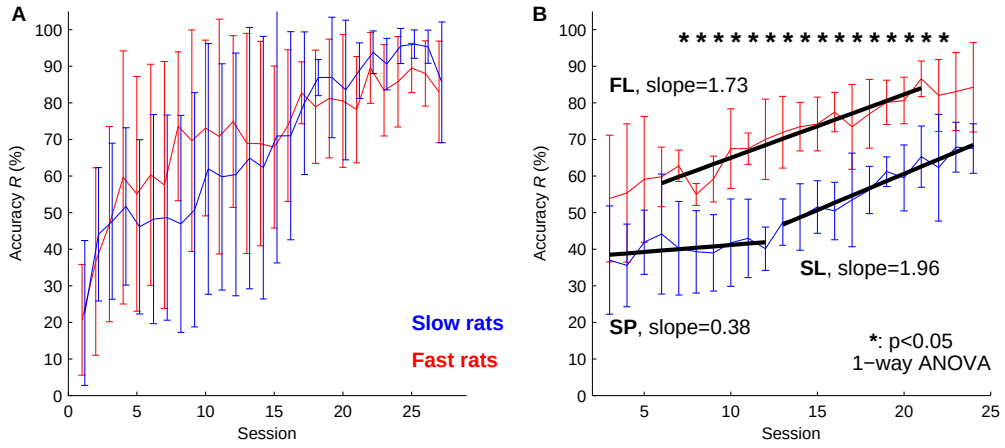

Figure 5.3: Behavioral performance in the training phase (A) and the learning phase (B). (A) The training accuracy of the first 28 sessions is shown for the fast and slow rats. Both groups of rats improved steadily and reached 80% in about 20 sessions. No significant difference was found between the training accuracy between the fast and slow rats. (B) The learning accuracy of session 3 to session 24 is shown for the fast and slow rats. The fast rats improved steadily while the slow rats started to improve from about 12 sessions on average. Three stages were identified for the fast and slow rats, respectively (see text). Three linear regression lines are provided for the FL, SP, and SL rats.

Single neuron firing rates were modulated by directional choice and previous trial outcome 5.4. Three types of firing rate modulation were therefore identified. First, the neurons were modulated by directional choice only (center panel of Fig. 5.4). Second, the neurons were modulated by previous trial outcome only (bottom panel of Fig. 5.4). Third, the neurons were modulated by both task factors (top panel of Fig. 5.4).

To ask if the neural activities were modulated by the two task factors in the neuron population, two-way ANOVA (directional control × previous trial outcome) was performed for fast and slow rats, respectively using a 200 ms window of a single trial timeline. Not many neurons (3.1%, average of the 3 task periods) show interactive

effects by the two task factors, which indicates that the two factors have independent effects in modulating firing rate. From the cue onset, fewer neurons in the fast rats were directional selective compared with slow rats (χ^2 test, $p < 0.05$; left panel of Fig. 5.5). However, more neurons were previous trial outcome selective in fast rats compared with slow rats in the cue-on period and even prior to the cue onset (χ^2 test, $p < 0.05$; right panel of Fig. 5.5).

Among the neurons with directional selectivity and/or previous trial outcome selectivity, a large portion of neurons were modulated by either previous trial outcome or directional choice (average of the cue on task period, slow rats: direction selective only, 38%; previous trial outcome selective only, 15%; fast rats, direction selective only, 16%; previous trial outcome selective only, 32%), while a few neurons showed selectivity for both (average of the cue on task period, 8% for slow rats, 15% for fast rats). This indicates that the two task factors were represented by separate groups of neurons.

5.3.4 Neural modulation by previous trial outcome

To investigate whether single units were differentially engaged in representing previous trial outcome for fast and slow rats, I analyzed the firing rate modulations by previous trial outcome measured I_1 (Fig. 5.6). The differences in firing rates between post-success and post-error trials were strongly affected by previous trial outcome in the cue-on data window. The averaged values of $|I_1|$ (top panel of Fig. 5.6) varied greatly from the pre-cue to the cue-on period, and they were the most prominent in the cue-on data window. The rate modulation was higher for fast group than the slow group.

To demonstrate changes in firing rates between fast and slow rats, I computed the $\bar{I}_1$ values in the cue-on data window for each neuron (Fig. 3B; slow: -0.1315 ± 0.1633;

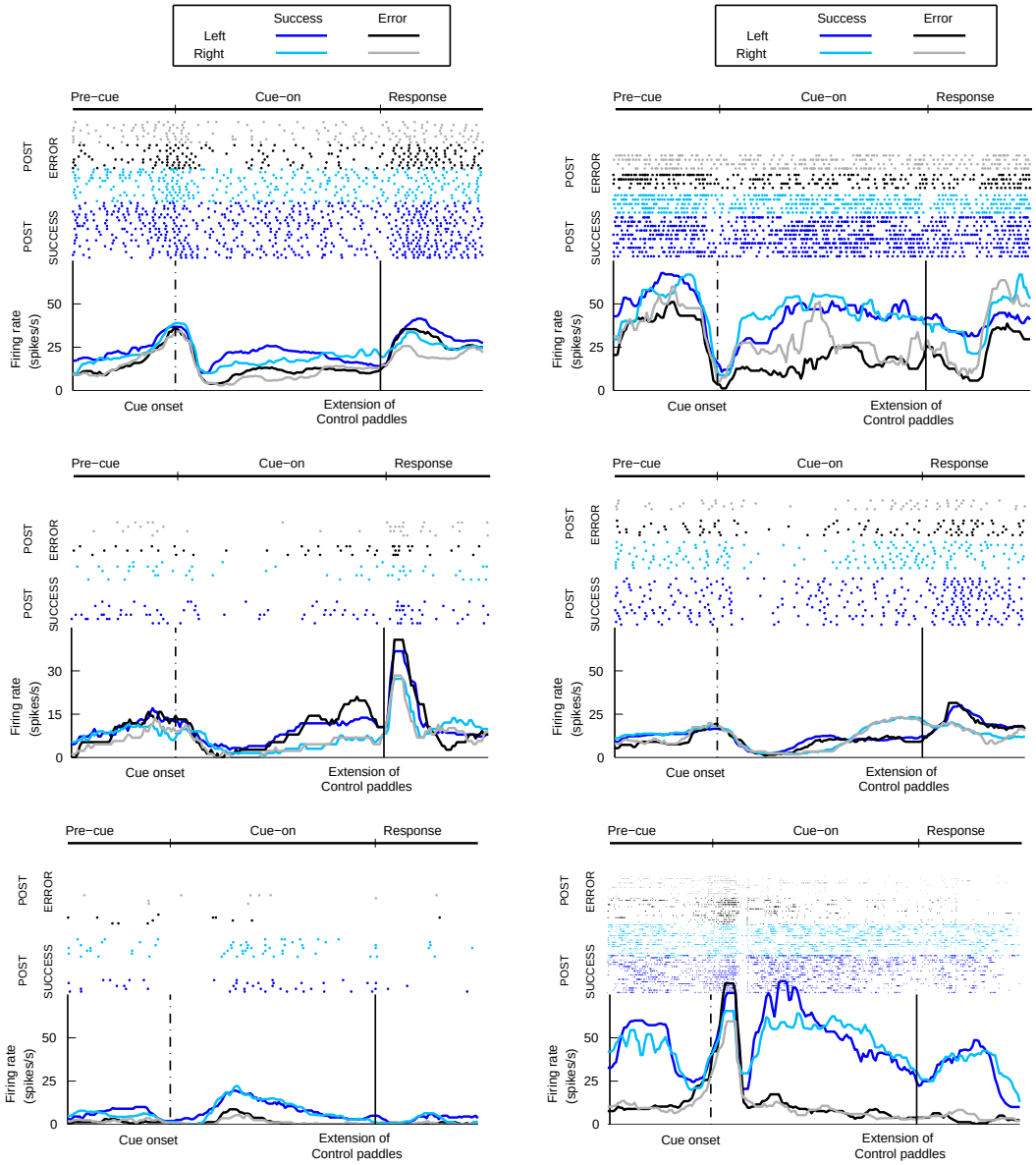

Figure 5.4: Neuronal representations reflecting previous trial outcome and directional choice. Example rasters and firing rates over trials of different movement directions and previous trial outcomes. Dark blue, the left press trials with previous trial outcome being successful. Light blue, the right press trials with previous trial being an error. Black, the left press trials with previous trial outcome being successful. Gray, the right press trials with previous trial being an error. Top left, rat D, channel 7, session 12. Top right, rat E, channel 14, session 16. Middle left, rat A, channel 12, session 12. Middle right, rat E, channel 7, session 11. Bottom left, rat H, channel 12, session 9. Bottom right, rat G, channel 16, session 16.

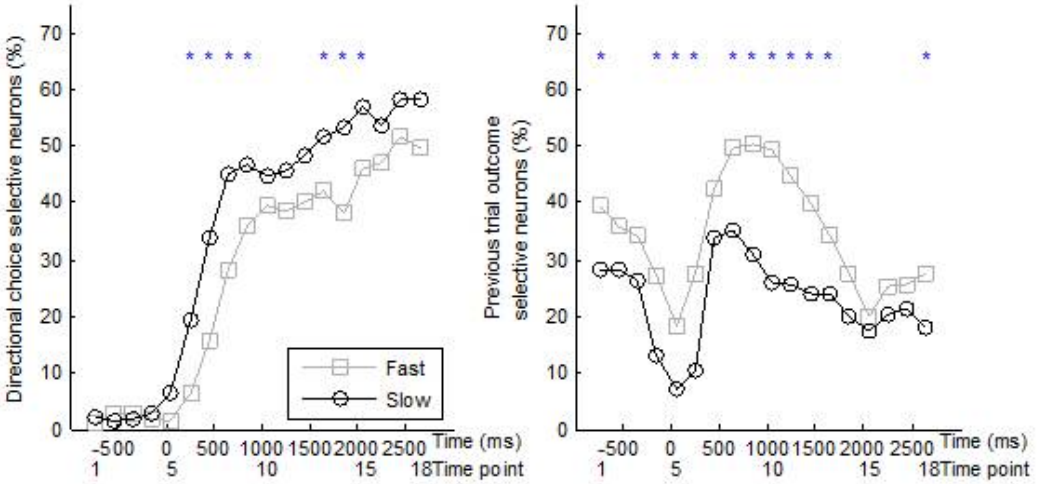

Figure 5.5: Fraction of neurons modulated by the two task factors in a trial timeline including three task periods. Blue asterisks indicate significant difference between the selective neuron fractions of fast and slow rats (χ^2 test, $p < 0.05$).

fast: -0.1767 ± 0.2118). The slow rats showed less firing rate differences between post-success and post-error trials than the fast rats.

Recall that $I_1 = \frac{(f_E(1)-f_S(1))}{(max(f_E(1),f_S(1)))}$. Overall, the finding that the $\bar{I_1}$ value was less than 0 for a large fraction of the units for fast (86%) and slow rats (75%). More neurons in the fast rats were associated with lower firing rates in post-error trials than in post-success trials, than compared with the slow rats.

5.3.5 Effect of previous trial outcome on directional selectivity

What is the effect of previous trial outcome on directional selectivity? To investigate, I compared the level of directional selectivity in post-error and post-success trials. The AUC values for directional choices were computed in post-error and post-success trials, respectively. The post-error trials had a more pronounced difference between left and right press trials than post-success trials in the fast rats (Fig. 5.7). This indicates that the post-error trials carried more information about directional

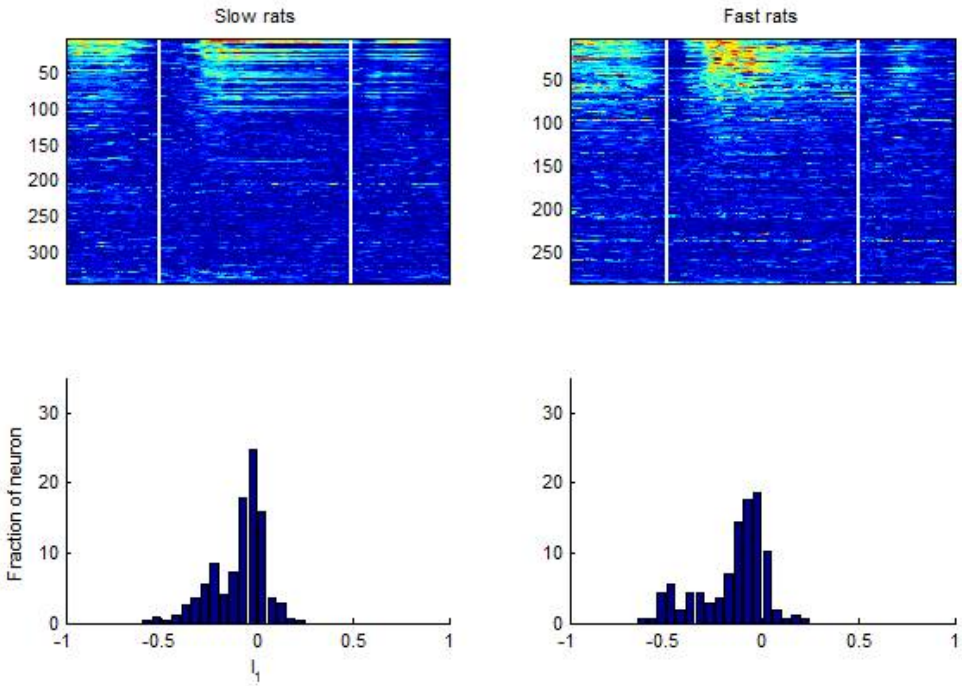

Figure 5.6: Modulation index of the previous trial outcomes for slow rats (left) and fast rats (right) in the cue-on data window. Top panel, the modulation index for all neurons recorded from slow rats (left) and fast rats (fast rats) in the pre-cue, cue-on, and response task periods. Bottom panel, $\bar{I}_1$ in the cue-on data window.

choice in the fast rats. However, for the slow rats, the directional selectivity in post-error and post-success trials does not differ.

5.4 Discussion

The work presented here makes a number of points about the learning process of fast and slow rats. First, although the rats were trained similarly and performed identical task, the fast rats and slow rats exhibited quite different learning curves. A group of fast rats achieved 70% steadily in a shorter time and on average showed higher 5-session learning slopes than the group of slow rats. Second, the neural activity in fast and slow rats differed when encoding previous trial outcome and

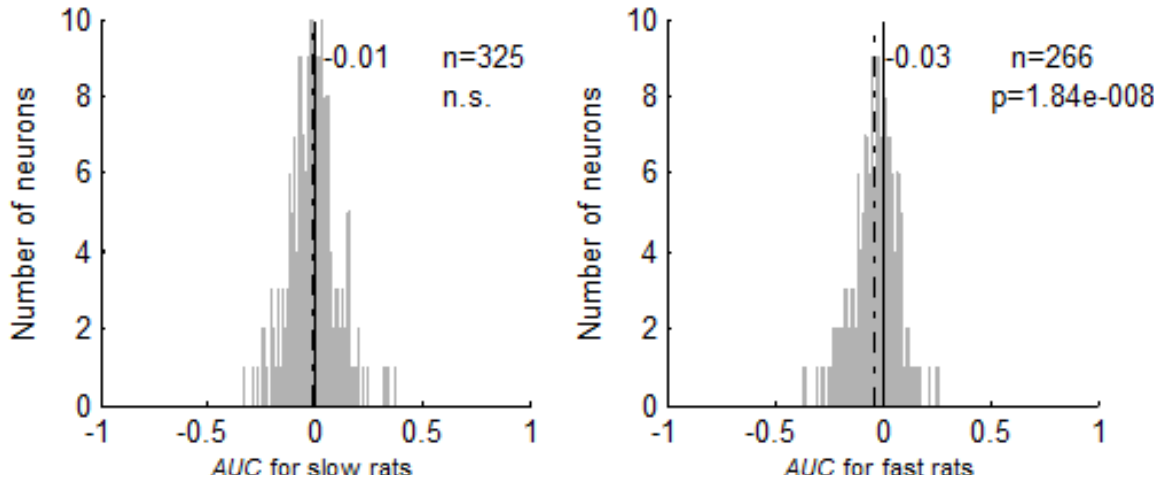

Figure 5.7: Histograms of AUC values showing difference in directional selectivity in post-error and post-success trials.

directional choice. The analysis based on neural data indicates that more neurons in the fast rats encoded previous trial outcome than the slow rats. The fast rats attended to the previous trial outcome more than the slow rats. The slow rats, on the other hand, did not pay attention to previous trial outcome and consequently resulted in poor learning performance.

Despite these differences in fast and slow rats, they also shared some common features. The fast rats and slow rats were handled and trained in the same way. Although the two groups of rats differed in learning performance, their training performance revealed no significant difference. This seems to indicate that rats were made of similar executive control capacity when they solve tasks that bear low cognitive load. Even though I have shown that the learning speed sets apart the fast rats from the slow rats, both slow and fast rats were able to improve their task performance and reached a performance accuracy of 70% or higher.

5.4.1 Learning from errors

Recent studies using rats and human subjects suggest that they may share similar traits in learning [120]. Learning relies on processing and integrating previous actions and feedbacks when making a new decision. Ohlsson proposed a theory of characterizing human learning from performance errors [119]. Error happens when the knowledge is available only in a general form. Such learning process contains two steps according to Ohlsson: error detection, and error correction. Recent research reveals that neural signals in humans medial frontal cortex (MFC) predict post-error adaptations. Changes in cognitive control performance can be predicted using error-related activity [134]. In another study, Hester and colleagues found individual differences in MFC activity also correlated with behavioral performance [135]. Human subjects with high levels of neural activity had better overall recall performance and higher error-correction rates. The MFC plays an indirect role in driving behavior change through its influence on other task-related regions.

5.4.2 Individual difference shown in neural activity

Individuals differ in their behavioral choices when they are confronted with decision uncertainty, develop elaborative strategies to learn a new task or skill [110], perform error-processing and introspective consciousness [117, 122, 123, 124], to name a few. Individuals also differ in reading abilities [125, 126]. Such differences may be influenced by age [122, 127, 128], sex [122, 129, 130, 131], genetic program [115] and intellectual abilities [110, 132]. However, in many experiments, individual difference is often omitted by averaging data across participants or subjects. Recently, the authors of [133] found that two monkeys, who were trained similarly and performed identical tasks, used different approaches when planning obstacle-avoidance reaches.

Also the decoding of population level firing activity suggests that neural activities in PMd activity are modulated by the particular planning strategy being used. In this study, two groups of rats performed the same task, while their learning characteristics were distinct.

In summary, individual differences, which may carry rich and important clues to neural information processing, are explored and exploited here to reveal the neural basis of higher order information processing task. Fast and slow rats showed difference in behavioral learning and neural activity. There may be a possible brain-behavior correlation between the neural activities encoding the previous trial outcome and the behavioral performance.

REFERENCES

[1] Chenhui Yang, Byron Olson, and Jennie Si. A multiscale correlation of wavelet coefficients approach to spike detection. *Neural. Comput.*, 23:215–250, 2011.

[2] P. G. Musial, S. N. Baker, G. L. Gerstein, E. A. King, and J. G. Keating. Signal-to-noise ratio improvement in multiple electrode recording. *J. Neurosci. Meth.*, 115:29–43, 2002.

[3] Michale S. Fee, Partha P. Mitra, and David Kleinfeld. Automatic sorting of multiple unit neuronal signals in the presence of anisotropic and non-gaussian variability. *J. Neurosci. Meth.*, 69:175–188, 1996.

[4] Quian R. Quiroga. Unsupervised spike detection and sorting with wavelets and superparamagnetic clustering. *Neural. Comput.*, 16:1661–1687, 2004.

[5] Frank Wood, Michael J. Black, Carlos Vargas-Irwin, Matthew Fellows, and John P. Donoghue. On the variability of manual spike sorting. *IEEE T Biomed. Eng.*, 51:912–918, 2004.

[6] T. Takekawa, Y. Isomura, , and T. Fukai. Accurate spike sorting for multi-unit recordings. *Eur. J. Neurosci.*, 31:263–272, 2010.

[7] Michael S Lewicki. A review of methods for spike sorting: the detection and classification of neural action potentials. *Network-comp. Neural.*, 9:R53–R78, 1998.

[8] E. Chah, V. Hok, A. Della-Chiesa, J. J. H. Miller, S. M. O'Mara, and R. B. Reilly. Automated spike sorting algorithm based on laplacian eigenmaps and k-means clustering. *J. Neural. Eng.*, 8:016006, 2011.

[9] Andreas K. Kreiter, Ad M.H.J. Aertsen, and George L. Gerstein. A low-cost single-board solution for real-time, unsupervised waveform classification of multineuron recordings. *J. Neurosci. Meth.*, 30(1):59–69, 1989.

[10] R.R. Harrison. A low-power integrated circuit for adaptive detection of action potentials in noisy signals. In *the 25th Annual Int. Conf. of the IEEE EMBS*, volume 4, pages 3325–3328, 2003.

[11] T Borghi, R Gusmeroli, A S Spinelli, and G Baranauskas. A simple method for efficient spike detection in multiunit recordings. *J. Neurosci. Meth.*, 163:176–180, 2007.

[12] Michael S Lewicki. Bayesian modeling and classification of neural signals. *Neural. Comput.*, 6:1005–1030, 1994.

[13] Shy Shoham, Matthew R. Fellows, and Matthew R. Fellows. Robust, automatic spike sorting using mixtures of multivariate t-distributions. *J. Neurosci. Meth.*, 127:111–122, 2003.

[14] J Eggermont, W Epping, and A Aertsen. Stimulus dependent neural correlations in the auditory midbrain of the grassfrog (rana temporaria l.). *Biol. Cybern.*, 47:103–120, 1983.

[15] Juan C. Letelier and Pamela P. Weber. Spike sorting based on discrete wavelet transform coefficients. *J. Neurosci. Meth.*, 101:93–106, 2000.

[16] Sunghan Kim and James McNames. Automatic spike detection based on adaptive template matching for extracellular neural recordings. *J. Neurosci. Meth.*, 165:165–174, 2007.

[17] Pu-Ming Zhang, Jin-Yong Wu, Yi Zhou, Pei-Ji Liang, and Jing-Qi Yuan. Spike sorting based on automatic template reconstruction with a partial solution to the overlapping problem. *J. Neurosci. Meth.*, 135:55–65, 2004.

[18] A.M. Haas, M.H. Cohen, and P.A. Abshire. Real-time variance based template matching spike sorting system. In *Life Science Systems and Applications Workshop*, 2007.

[19] Scott B. Wilsona, Christine A. Turnerb, Ronald G. Emersonb, and Mark L. Scheuer. Spike detection ii: automatic, perception-based detection and clustering. *Clin. Neurophysiol.*, 110:404–411, 1999.

[20] Susumu Takahashi, Yuichiro Anzai, and Yoshio Sakurai. A new approach to spike sorting for multi-neuronal activities recorded with a tetrode–how ica can be practical. *Neurosci. Res.*, 46:265–272, 2003.

[21] Zoran Nenadic and Joel W. Burdick. Spike detection using the continuous wavelet transform. *IEEE T Biomed. Eng.*, 52:74–87, 2005.

[22] Kyung Hwan Kim and Sung June Kim. A wavelet-based method for action potential detection from extracellular neural signal recording with low signal-to-noise ratio. *IEEE T Biomed. Eng.*, 50:999–1011, 2003.

[23] Yuan Yuan, Chenhui Yang, and Jennie Si. An advanced spike detection and sorting system. In *IJCNN*, volume 4, pages 3325–3328, 2009.

[24] Edward M. Schmidt and Donald R. Humphrey. *Neurophysiological Techniques: Applications to Neural Systems*. Humana Press, 1990.

[25] Gang Wu, Rolf G. Hallin, and Rolf Ekedahl. Multiple action potential waveforms of single units in man as signs of variability in conductivity of their myelinated fibres. *Brain Res*, 742(12):225–238, 1996.

[26] Eyal Hulata, Ronen Segev, Yoash Shapira, Morris Benveniste, and Eshel Ben-Jacob. Detection and sorting of neural spikes using wavelet packets. *Phys Rev Lett*, 2000.

[27] Eyal Hulata, Ronen Segev, and Eshel Ben-Jacob. A method for spike sorting and detection based on wavelet packets and shannon's mutual information. *J. Neurosci. Meth.*, 2002.

[28] L. Smith. Noisy spike generator, matlab software, 2006. Available at `http://www.cs.stir.ac.uk/ lss/noisyspikes/`.

[29] Cameron S Carter, Todd S Braver, Deanna M Barch, Matthew M Botvinick, Douglas Noll, and Jonathan D Cohen. Anterior cingulate cortex, error detection, and the online monitoring of performance. *Science*, 280(5364):747–749, 1998.

[30] Veit Stuphorn, Tracy L Taylor, and Jeffrey D Schall. Performance monitoring by the supplementary eye field. *Nature*, 408(6814):857–860, 2000.

[31] Jeffrey D Schall, Veit Stuphorn, and Joshua W Brown. Monitoring and control of action by the frontal lobes. *Neuron*, 36(2):309–322, 2002.

[32] Hein T van Schie, Rogier B Mars, Michael GH Coles, and Harold Bekkering. Modulation of activity in medial frontal and motor cortices during error observation. *Nature neuroscience*, 7(5):549–554, 2004.

[33] Jose L Pardo-Vazquez, Victor Leboran, and Carlos Acuña. Neural correlates of decisions and their outcomes in the ventral premotor cortex. *The Journal of Neuroscience*, 28(47):12396–12408, 2008.

[34] Harry Uylings, Henk J Groenewegen, and Bryan Kolb. Do rats have a prefrontal cortex? *Behavioural brain research*, 146(1):3–17, 2003.

[35] Nathaniel J Smith, Nicole K Horst, Benjamine Liu, Marcelo S Caetano, and Mark Laubach. Reversible inactivation of rat premotor cortex impairs temporal preparation, but not inhibitory control, during simple reaction-time performance. *Frontiers in integrative neuroscience*, 4, 2010.

[36] Jung Hoon Sul, Suhyun Jo, Daeyeol Lee, and Min Whan Jung. Role of rodent secondary motor cortex in value-based action selection. *Nature neuroscience*, 14(9):1202–1208, 2011.

[37] Mark Laubach, Johan Wessberg, and Miguel AL Nicolelis. Cortical ensemble activity increasingly predicts behaviour outcomes during learning of a motor task. *Nature*, 405(6786):567–571, 2000.

[38] EJ Neafsey and Carl Sievert. A second forelimb motor area exists in rat frontal cortex. *Brain research*, 232(1):151–156, 1982.

[39] John P Donoghue and Steven P Wise. The motor cortex of the rat: cytoarchitecture and microstimulation mapping. *Journal of Comparative Neurology*, 212(1):76–88, 1982.

[40] RE Passingham, C Myers, N Rawlins, V Lightfoot, and S Fearn. Premotor cortex in the rat. *Behavioral neuroscience*, 102(1):101, 1988.

[41] RL Reep, GS Goodwin, and JV Corwin. Topographic organization in the corticocortical connections of medial agranular cortex in rats. *Journal of Comparative Neurology*, 294(2):262–280, 1990.

[42] Jeffrey W Dalley, Rudolf N Cardinal, and Trevor W Robbins. Prefrontal executive and cognitive functions in rodents: neural and neurochemical substrates. *Neuroscience & Biobehavioral Reviews*, 28(7):771–784, 2004.

[43] RL Reep, JV Corwin, and A Hashimoto and RT Watson. Efferent connections of the rostral portion of medial agranular cortex in rats. *Brain research bulletin*, 19(2):203–221, 1987.

[44] Jeffrey A Kleim, Scott Barbay, and Randolph J Nudo. Functional reorganization of the rat motor cortex following motor skill learning. *Journal of Neurophysiology*, 80(6):3321–3325, 1998.

[45] Jerome N Sanes and John P Donoghue. Plasticity and primary motor cortex. *Annual review of neuroscience*, 23(1):393–415, 2000.

[46] Adam F Carpenter, Apostolos P Georgopoulos, and Giuseppe Pellizzer. Motor cortical encoding of serial order in a context-recall task. *Science*, 283(5408):1752–1757, 1999.

[47] Yoshiya Matsuzaka, Nathalie Picard, and Peter L Strick. Skill representation in the primary motor cortex after long-term practice. *Journal of neurophysiology*, 97(2):1819–1832, 2007.

[48] G Kartje-Tillotson, EJ Neafsey, and AJ Castro. Electrophysiological analysis of motor cortical plasticity after cortical lesions in newborn rats. *Brain research*, 332(1):103–111, 1985.

[49] RJ Nudo, WM Jenkins, and MM Merzenieh. Repetitive microstimulation alters the cortical representation of movements in adult rats. *Somatosensory & motor research*, 7(4):463–483, 1990.

[50] Apostolos P Georgopoulos. Neural aspects of cognitive motor control. *Current Opinion in Neurobiology*, 10(2):238–241, 2000.

[51] Riccardo Viaro, Michele Morari, and Gianfranco Franchi. Progressive motor cortex functional reorganization following 6-hydroxydopamine lesioning in rats. *The Journal of Neuroscience*, 31(12):4544–4554, 2011.

[52] Martine R van Schouwenburg, Jacinta O'Shea, Rogier B Mars, Matthew FS Rushworth, and Roshan Cools. Controlling human striatal cognitive function via the frontal cortex. *The Journal of Neuroscience*, 32(16):5631–5637, 2012.

[53] D Huber, DA Gutnisky, S Peron, DH OConnor, JS Wiegert, L Tian, TG Oertner, LL Looger, and K Svoboda. Multiple dynamic representations in the motor cortex during sensorimotor learning. *Nature*, 484(7395):473–478, 2012.

[54] Andrew R Mitz, Moshe Godschalk, and Steven P Wise. Learning-dependent neuronal activity in the premotor cortex: activity during the acquisition of conditional motor associations. *The Journal of neuroscience*, 11(6):1855–1872, 1991.

[55] Jonathan D Wallis and Earl K Miller. From rule to response: neuronal processes in the premotor and prefrontal cortex. *Journal of Neurophysiology*, 90(3):1790–1806, 2003.

[56] George Paxinos and Charles Watson. *The rat brain in stereotaxic coordinates: hard cover edition*. Access Online via Elsevier, 2004.

[57] Yuan Yuan, Chenhui Yang, and Jennie Si. The m-sorter: An automatic and robust spike detection and classification system. *Journal of Neuroscience Methods*, 210:281–290, 2012.

[58] David Marvin Green, John A Swets, et al. *Signal detection theory and psychophysics*, volume 1. Wiley New York, 1966.

[59] Kenneth H Britten, Michael N Shadlen, William T Newsome, and J Anthony Movshon. The analysis of visual motion: a comparison of neuronal and psychophysical performance. *The Journal of Neuroscience*, 12(12):4745–4765, 1992.

[60] Adam S Dickey, Aaron Suminski, Yali Amit, and Nicholas G Hatsopoulos. Single-unit stability using chronically implanted multielectrode arrays. *Journal of neurophysiology*, 102(2):1331–1339, 2009.

[61] Andrew Jackson and Eberhard E Fetz. Compact movable microwire array for long-term chronic unit recording in cerebral cortex of primates. *Journal of Neurophysiology*, 98(5):3109–3119,2007.

[62] Nandakumar S Narayanan and Mark Laubach. Delay activity in rodent frontal cortex during a simple reaction time task. *Journal of neurophysiology*, 101(6):2859–2871, 2009.

[63] Thomas Michelet, Bernard Bioulac, Dominique Guehl, Michel Goillandeau, and Pierre Burbaud. Single medial prefrontal neurons cope with error. *PLos ONE*, 4(7):e6240, 2009.

[64] Claudia Danielmeier, Tom Eichele, Birte U Forstmann, Marc Tittgemeyer, and Markus Ullsperger. Posterior medial frontal cortex activity predicts post-error adaptations in task-related visual and motor areas. *The Journal of Neuroscience*, 31(5):1780–1789, 2011.

[65] Apostolos P Georgopoulos, John F Kalaska, Roberto Caminiti, and Joe T Massey. On the relations between the direction of two-dimensional arm movements and cell discharge in primate motor cortex. *The Journal of Neuroscience*, 2(11):1527–1537, 1982.

[66] Daniel W Moran and Andrew B Schwartz. Motor cortical representation of speed and direction during reaching. *Journal of Neurophysiology*, 82(5):2676–2692, 1999.

[67] Sylvia Wirth, Emin Avsar, Cindy C Chiu, Varun Sharma, Anne C Smith, Emery Brown, Wendy A Suzuki. Trial outcome and associative learning signals in the monkey hippocampus. *Neuron*, 61:930-940, 2009.

[68] Christopher H Donahue, Hyojung Seo, Daeyeol Lee. Cortical Signals for Rewarded Actions and Strategic Exploration. *Neuron*, 80(1):223–234, 2013.

[69] Claudia Danielmeier, Tom Eichele, Birte U Forstmann, Marc Tittgemeyer, Markus Ullsperger. Posterior medial frontal cortex activity predicts post-error adaptations in task-related visual and motor areas. *The Journal of Neuroscience*, 31(5):1780–1789, 2011.

[70] Hyojung Seo, Dominic J Barraclough, Daeyeol Lee. Dynamic signals related to choices and outcomes in the dorsolateral prefrontal cortex. *Cerebral Cortex*, 17(suppl 1):i110–i117, 2007.

[71] Rene Quilodran, Marie Rothe, Emmanuelyeol Procyk. Behavioral shifts and action valuation in the anterior cingulate cortex. *Neuron*, 57(2):314–325, 2008.

[72] Clay B Holroyd and Michael GH Coles. The neural basis of human error processing: reinforcement learning, dopamine, and the error-related negativity. *Psychological review*, 109(4):679, 2002.

[73] Mengia-S Rioult-Pedotti, Daniel Friedman, Grzegorz Hess, John P Donoghue. Strengthening of horizontal cortical connections following skill learning. *Nature neuroscience*, 1(2):230–234, 1998.

[74] Michael S Remple and Jamie L Jamie and Iwona Stepniewska and David C Lyon and Jon H Kaas. The organization of frontoparietal cortex in the tree shrew (Tupaia belangeri): II. Connectional evidence for a frontal-posterior parietal network. *Journal of Comparative Neurology*, 501(1):121–149, 2007.

[75] Todd M Preuss. Do rats have prefrontal cortex? The Rose-Woolsey-Akert program reconsidered. *Journal of Cognitive Neuroscience*, 7(1):1–24, 1995.

[76] Yoshifumi Ueta and Takeshi Otsuka and Mieko Morishima and Mika Ushimaru and Yasuo Kawaguchi. Multiple layer 5 pyramidal cell subtypes relay cortical feedback from secondary to primary motor areas in rats. *Cerebral Cortex*, 501(1):121–149, 2013.

[77] Johnp P Donoghue and Carol Parham. Afferent connections of the lateral agranular field of the rat motor cortex. *Journal of Comparative Neurology*, 217(4):390–404, 1983.

[78] Susan R Sesack and Ariel Y Deutch and Robert H Roth and Benjamin S Bunney. Topographical organization of the efferent projections of the medial prefrontal cortex in the rat: An anterograde tract-tracing study with Phaseolus vulgaris leucoagglutinin. *Journal of Comparative Neurology*, 290(2):213–242, 1989.

[79] RE Passingham and C Myers and N Rawlins and V Lightfoot and S Fearn. Premotor cortex in the rat. *Behavioral neuroscience*, 102(1):101, 1988.

[80] Verity J Brown and Eric M Bowman. Rodent models of prefrontal cortical function. *Trends in neurosciences*, 25(7):340–343, 2002.

[81] HBM Uylings and CG Van Eden. Qualitative and quantitative comparison of the prefrontal cortex in rat and in primates, including humans. *Prog Brain Res*, 85:31–62, 1990.

[82] Françoise Condé and Evelyne Maire-lepoivre and Etienne Audinat and Francis Crepel. Afferent connections of the medial frontal cortex of the rat. II. Cortical and subcortical afferents. *Journal of Comparative Neurology*, 352(4):567–593, 1995.

[83] Dan Hu and Abram Amsel. A simple test of the vicarious trial-and-error hypothesis of hippocampal function. *Proceedings of the National Academy of Sciences*, 92(12):5506–5509, 1995.

[84] GV Hamilton. A study of trial and error reactions in mammals. *Journal of Animal Behavior*, 1(1):33, 1911.

[85] Greg Hajcak, Nicole McDonald, and Robert F Simons. To err is autonomic: Error-related brain potentials, ans activity, and post-error compensatory behavior. *Psychophysiology*, 40(6):895–903, 2003.

[86] Matthew R. Roesch and Carl R. Olson. Impact of expected reward on neuronal activity in prefrontal cortex, frontal and supplementary eye fields and premotor cortex. *Journal of Neurophysiology*, 90:1766–1789, 2003.

[87] Shunsuke Kobayashi, Kensaku Nomoto, Masataka Watanabe, Okihide Hikosaka, Wolfram Schultz, and Masamichi Sakagami. Influences of rewarding and aversive outcomes on activity in macaque lateral prefrontal cortex. *Neuron.*, 51:861–870, 2006.

[88] Daeyeol Lee and Hyojung Seo. Mechanisms of reinforcement learning and decision making in the primate dorsolateral prefrontal cortex. *Ann. N.Y. Acad. Sci.*, 1104:108–122, 2007.

[89] Hyojung Seo and Daeyeol Lee. Temporal filtering of reward signals in the dorsal anterior cingulate cortex during a mixed-strategy game. *J. Neurosci.*, 27:8366–8377, 2007.

[90] Kathrin Koch, Claudia Schachtzabel, Gerd Wagner, Jurgen R. Reichenbach, Heinrich Sauer, and Ralf Schlosser. The neural correlates of reward-related trial-and-error learning: An fmri study with a probabilistic learning task. *Learning Memory*, 15:728–732, 2008.

[91] Nandakumar S Narayanan and Mark Laubach. Neuronal correlates of post-error slowing in the rat dorsomedial prefrontal cortex. *Journal of neurophysiology*, 100(1):520–525, 2008.

[92] Mark H Histed, Anitha Pasupathy, and Earl K Miller. Learning substrates in the primate prefrontal cortex and striatum: sustained activity related to successful actions. *Neuron*, 63(2):244–253, 2009.

[93] Steven W. Kennerley and Jonathan D. Wallis. Reward-dependent modulation of working memory in lateral prefrontal cortex. *Journal of Neuroscience*, 29:3259–3270, 2009.

[94] Michael Falkenstein, Horst Hielscher, Isabel Dziobek, Paul Schwarzenau, Jörg Hoormann, Brigitte Sundermann, and Joachim Hohnsbein. Action monitoring, error detection, and the basal ganglia: an erp study. *Neuroreport*, 12(1):157–161, 2001.

[95] Daniela Vallentin, Sylvia Bongard, and Andreas Nieder. Numerical rule coding in the prefrontal, premotor, and posterior parietal cortices of macaques. *The Journal of Neuroscience*, 32(19):6621–6630, 2012.

[96] van CG Eden, VAF Lamme, and HBM Uylings. Heterotopic cortical afferents to the medial prefrontal cortex in the rat. a combined retrograde and anterograde tracer study. *European Journal of Neuroscience*, 4(1):77–97, 1992.

[97] Paul LA Gabbott, Tracy A Warner, Paul RL Jays, Phillip Salway, and Sarah J Busby. Prefrontal cortex in the rat: projections to subcortical autonomic, motor, and limbic centers. *Journal of Comparative Neurology*, 492(2):145–177, 2005.

[98] Walter B Hoover and Robert P Vertes. Anatomical analysis of afferent projections to the medial prefrontal cortex in the rat. *Brain Structure and Function*, 212(2):149–179, 2007.

[99] C Acuña, JL Pardo-Vazquez, and V Leboran. Decision-making, behavioral supervision and learning: an executive role for the ventral premotor cortex? *Neurotoxicity research*, 18(3-4):416–427, 2010.

[100] Jose L Pardo-Vazquez, Victor Leboran, and Carlos Acuña. A role for the ventral premotor cortex beyond performance monitoring. *Proceedings of the National Academy of Sciences*, 106(44):18815–18819, 2009.

[101] Tobias Egner and Joy Hirsch. Cognitive control mechanisms resolve conflict through cortical amplification of task-relevant information. *Nature neuroscience*, 8(12):1784–1790, 2005.

[102] Josep Marco-Pallarés, Estela Camara, Thomas F Münte, and Antoni Rodríguez-Fornells. Neural mechanisms underlying adaptive actions after slips. *Journal of cognitive neuroscience*, 20(9):1595–1610, 2008.

[103] Jared B Smith and Kevin D Alloway. Rat whisker motor cortex is subdivided into sensory-input and motor-output areas. *Frontiers in neural circuits*, 7, 2013.

[104] JA Hosp, K Molina-Luna, B Hertler, C Osei Atiemo, and AR Luft. Dopaminergic modulation of motor maps in rat motor cortex: An in vivo study. *Neuroscience*, 159(2):692–700, 2009.

[105] Andreas R Luft and Stefanie Schwarz. Dopaminergic signals in primary motor cortex. *International Journal of Developmental Neuroscience*, 27(5):415–421, 2009.

[106] HJ Groenewegen and MP Witter. Thalamus. *The rat nervous system*, 3:407–453, 2004.

[107] Janaina Pantoja, Sidarta Ribeiro, Michael Wiest, Ernesto Soares, Damien Gervasoni, Nelson AM Lemos, and Miguel AL Nicolelis. Neuronal activity in the primary somatosensory thalamocortical loop is modulated by reward contingency during tactile discrimination. *The Journal of Neuroscience*, 27(39):10608–10620, 2007.

[108] Takashi Kawagoe, Ryoi Tamura, Teruko Uwano, Takashi Asahi, Hisao Nishijo, Satoshi Eifuku, and Taketoshi Ono. Neural correlates of stimulus-reward association in the rat mediodorsal thalamus. *Neuroreport*, 18(7):683–688, 2007.

[109] Burkhard Pleger, Christian C Ruff, Felix Blankenburg, Stefan Klöppel, Jon Driver, and Raymond J Dolan. Influence of dopaminergically mediated reward on somatosensory decision-making. *PLoS biology*, 7(7):e1000164, 2009.

[110] Alvin Y Wang. Individual differences in learning speed. *Journal of Experimental Psychology: Learning, Memory, and Cognition*, 9(2):300, 1983.

[111] Henry H Yin, Shweta Prasad Mulcare, Monica RF Hilário, Emily Clouse, Terrell Holloway, Margaret I Davis, Anita C Hansson, David M Lovinger, and Rui M Costa. Dynamic reorganization of striatal circuits during the acquisition and consolidation of a skill. *Nature neuroscience*, 12(3):333–341, 2009.

[112] William J Kargo and Douglas A Nitz. Improvements in the signal-to-noise ratio of motor cortex cells distinguish early versus late phases of motor skill learning. *The Journal of neuroscience*, 24(24):5560–5569, 2004.

[113] Linda Hermer-Vazquez and Nasim Moshtagh. Rats learning of a new motor skill: Insight into the evolution of motor sequence learning. *Behavioural processes*, 81(1):50–59, 2009.

[114] Richard J Haier, Benjamin Siegel, Chuck Tang, Lennart Abel, and Monte S Buchsbaum. Intelligence and changes in regional cerebral glucose metabolic rate following learning. *Intelligence*, 16(3):415–426, 1992.

[115] Michael J Frank, Bradley B Doll, Jen Oas-Terpstra, and Francisco Moreno. Prefrontal and striatal dopaminergic genes predict individual differences in exploration and exploitation. *Nature neuroscience*, 12(8):1062–1068, 2009.

[116] Bharat B Biswal, Dana A Eldreth, Michael A Motes, and Bart Rypma. Task-dependent individual differences in prefrontal connectivity. *Cerebral Cortex*, 20(9):2188–2197, 2010.

[117] Stephen M Fleming, Rimona S Weil, Zoltan Nagy, Raymond J Dolan, and Geraint Rees. Relating introspective accuracy to individual differences in brain structure. *Science*, 329(5998):1541–1543, 2010.

[118] Ryota Kanai and Geraint Rees. The structural basis of inter-individual differences in human behaviour and cognition. *Nature Reviews Neuroscience*, 12(4):231–242, 2011.

[119] Stellan Ohlsson. Learning from performance errors. *Psychological review*, 103(2):241, 1996.

[120] Robin A Murphy, Esther Mondragón, and Victoria A Murphy. Rule learning by rats. *Science*, 319(5871):1849–1851, 2008.

[121] Dana Cohen and Miguel AL Nicolelis. Reduction of single-neuron firing uncertainty by cortical ensembles during motor skill learning. *The Journal of neuroscience*, 24(14):3574–3582, 2004.

[122] Robert Hester, Catherine Fassbender, and Hugh Garavan. Individual differences in error processing: a review and reanalysis of three event-related fmri studies using the go/nogo task. *Cerebral Cortex*, 14(9):986–994, 2004.

[123] Maarten AS Boksem, Mattie Tops, Anne E Wester, Theo F Meijman, and Monicque M Lorist. Error-related erp components and individual differences in punishment and reward sensitivity. *Brain research*, 1101(1):92–101, 2006.

[124] A Eve Miller, Jason M Watson, and David L Strayer. Individual differences in working memory capacity predict action monitoring and the error-related negativity. *Journal of Experimental Psychology: Learning, Memory, and Cognition*, 38(3):757, 2012.

[125] Meredyth Daneman and Patricia A Carpenter. Individual differences in working memory and reading. *Journal of verbal learning and verbal behavior*, 19(4):450–466, 1980.

[126] Jonathan King and Marcel Adam Just. Individual differences in syntactic processing: The role of working memory. *Journal of memory and language*, 30(5):580–602, 1991.

[127] Cheryl L Grady, Jose Ma Maisog, Barry Horwitz, Leslie G Ungerleider, MJ Mentis, JA Salerno, P Pietrini, E Wagner, and JV Haxby. Age-related changes in cortical blood flow activation during visual processing of faces and location. *The Journal of Neuroscience*, 14(3):1450–1462, 1994.

[128] Lars Nyberg, Lars-Göran Nilsson, Ulrich Olofsson, and Lars Bäckman. Effects of division of attention during encoding and retrieval on age differences in episodic memory. *Experimental aging research*, 23(2):137–143, 1997.

[129] William DS Killgore, Mika Oki, and Deborah A Yurgelun-Todd. Sex-specific developmental changes in amygdala responses to affective faces. *Neuroreport*, 12(2):427–433, 2001.

[130] William DS Killgore and Deborah A Yurgelun-Todd. Sex differences in amygdala activation during the perception of facial affect. *Neuroreport*, 12(11):2543–2547, 2001.

[131] Susan L Rossell, Edward T Bullmore, Steve CR Williams, and Anthony S David. Sex differences in functional brain activation during a lexical visual field task. *Brain and language*, 80(1):97–105, 2002.

[132] Phillip L Ackerman and Anna T Cianciolo. Cognitive, perceptual-speed, and psychomotor determinants of individual differences during skill acquisition. *Journal of Experimental Psychology: Applied*, 6(4):259, 2000.

[133] Thomas M Pearce and Daniel W Moran. Strategy-dependent encoding of planned arm movements in the dorsal premotor cortex. *Science*, 337(6097):984–988, 2012.

[134] Robert Hester, Janelle Madeley, Kevin Murphy, and Jason B Mattingley. Learning from errors: error-related neural activity predicts improvements in future inhibitory control performance. *The Journal of Neuroscience*, 29(22):7158–7165, 2009.

[135] Robert Hester, Natalie Barre, Kevin Murphy, Tim J Silk, and Jason B Mattingley. Human medial frontal cortex activity predicts learning from errors. *Cerebral Cortex*, 18(8):1933–1940, 2008.